Extraction and separation of rare earth elements from hydrothermal metalliferous sediments

Pierre Josso, Steve Roberts, Damon A.H. Teagle, Olivier Pourret, Richard Herrington, Carlos Ponce de Leon Albarran

Extraction and separation of rare earth elements from hydrothermal metalliferous sediments.

Pierre Josso[1], Steve Roberts[1], Damon A. H. Teagle[1], Olivier Pourret[2], Richard Herrington[3], Carlos Ponce de Leon Albarran[4]

[1]Ocean and Earth Science, National Oceanography Centre Southampton, University of Southampton, Southampton, SO14 3ZH, UK.

[2]UniLaSalle, AGHYLEm 60026 Beauvais cedex, France

[3]Department of Earth Sciences, Natural History Museum, London SW7 5BD, UK

[4]Electrochemical Engineering Laboratory, Energy Technology Research Group, University of Southampton, Highfield, Southampton, UK

Corresponding author: Pierre Josso (piesso@bgs.ac.uk) ORCID: 0000-0003-3819-4536
Postal: British Geological Survey, Environmental Science Centre, Keyworth, Nottingham NG12 5GG.

Abstract

Rare earth elements (REE) can be efficiently extracted from umbers, ferromanganese metalliferous sediments of the Troodos ophiolite (Cyprus) by simple leaching and selective precipitation, without accumulation of radioactive by-products. Umbers are dominantly composed of amorphous Fe and Mn oxides with minor goethite, quartz and zeolites, and contain 350 – 500 $mg.kg^{-1}$ of rare earth elements and yttrium (REY), 200 times lower than many of the major REY source ores. To compensate for relatively low grades, a cost-effective extraction process was developed that utilises a weak lixiviant concentration (0.1 – 1.5 N) and short reaction times (5 min to 11 h). Acid solutions recover 70-85% of the initial sample REY content even at 20 °C. By contrast, extraction using ionic solutions of NaCl and ammonium sulphate proved ineffective. Acid recoveries of REY increase by nearly 10% at 70 °C and the use of different acids (HCl, HNO_3, H_2SO_4) yields comparable results. The main impurities in the leachate include Ca and Na at even the weakest acid concentration (0.1 N). However, two-step leaching method greatly reduces concentrations of impurities in the REY-rich liquor, although with REY losses approaching 20%. Purification of the leach liquor via selective precipitation of REY as an oxalate is highly efficient although pH dependent. With maximum REY precipitation (96-99%) occurring between pH 1 and 2, the precise adjustment of pH allows separation of REY from other precipitating impurities (Ca). The maximum purity of the precipitate is achieved at pH 1.1 (> 65%). Strong and consistent fractionation along the lanthanide series observed during the precipitation experiments has been successfully explained using a speciation modelling software (PHREEQC). The uptake of REY by oxalate in the experiments closely follows the bell-shape distribution of REY-oxalate solid complexes stability constant (-log β ($RE_2Ox_3.nH_2O$)) replicating the fractionation trends observed at pH < 1.1. In addition, the modelling demonstrates that at equivalent REE concentration in solution, oxalate precipitates fractionate REY in the following order: middle REE > light REE >> heavy REE. This ordering and the variable degrees of uptake reflects the interplay of aqueous REY-oxalate complexes (log $_{HOx}\beta_1$, $_{Ox}\beta_1$ and $_{Ox}\beta_2$) with the natural fractionation induced by solid REY-oxalate stability constant distribution. Overall, the combined leaching process and selective oxalate precipitation produces a total enrichment factor ranging between 1400 and 2400 for REY from the sample to the oxalate precipitate in a simple two-step process forming a high-purity end-product of mixed REY.

Keywords: leaching; metalliferous sediments; oxalate; PHREEQC; rare earth elements; speciation modelling; umbers.

1. Introduction

The perceived supply risk for essential materials used in the development of green energy and other state-of-the art technologies provides motivation to investigate new sources for these raw materials. Many are characterized as "critical", given supply risks posed by geographic location, the economic and political stability of producing countries, limited possibilities for substitution and currently low-levels of recycling (European Commission, 2014, Graedel *et al.*, 2014). At present, 20 raw materials are listed by the European Union as critical. Among these critical elements, the lanthanides and yttrium (REY) form a group of 15 metals (Rollat *et al.*, 2016) essential for the development of applications in the low-carbon energy sector (magnets, low-energy lighting, wind turbines, batteries), industry (catalysis, alloys, oil refining), and other technologies (lasers, optics) (Guyonnet *et al.*, 2015). More than 90% of REY produced worldwide in the last twenty years originated in China, a near monopoly that reflects environmental and economic factors rather than the unequal distribution of REY resources across the world (Weng *et al.*, 2015). Indeed, large primary deposits are known outside China including more than 550 carbonatites/alkaline complexes worldwide (Kanazawa and Kamitani, 2006, Chakhmouradian and Wall, 2012, Jordens *et al.*, 2013, Jaireth *et al.*, 2014, Xie *et al.*, 2014, Hoshino *et al.*, 2016).

Solvent extraction constitutes the most common treatment of REE-bearing minerals, such as xenotime (YPO_4), bastnäsite ($(Ce,La)CO_3F$) and monazite ($(REE,Th)PO_4$) ores, following energy-consuming beneficiation via gravity separation, desliming, magnetic or electrostatic separation and froth flotation (Jordens et al., 2013, Kumar *et al.*, 2014, Xie et al., 2014). The hydrometallurgical process uses strong acid or alkali leaches (sulphuric acid and sodium hydroxide being the most common) at temperatures of 200-400 °C, in a process commonly referred to as cracking (Habashi, 2013, Golev *et al.*, 2014). This treatment produces REE-rich leach liquors usually in the range of 1 to 40 $g.L^{-1}$ RE_2O_3 with small amounts of impurities (Chi *et al.*, 1995, Abreu and Morais, 2010). REY are separated from co-leached elements by further treatment such as solvent extraction and ion exchange using selective precipitation as carbonates or oxalates by pH adjustment. Rare earth oxalates and carbonates are then roasted to form a mixed RE oxide product ready for sale as a RE alloy known as mischmetal, sent to specialized factories for further separation treatment into individual high purity RE oxides or reduced to pure metal products depending on the required end use (Christie *et al.*, 1998, Golev et al., 2014). The separation of a mixed product into individual elements is inherently difficult due to their very similar chemical behaviour. Multiple methods exist such as selective oxidation/reduction, fractional crystallisation-precipitation, and ion-exchange, though the most effective approach is solvent extraction using organophosphorus compounds (e.g, EDPA, HDEHP, EHEHPA, or TBP) (Abreu and Morais, 2014, Kumar et al., 2014, Xie et al., 2014). All these methods are energy- and material-consuming as they require multiple iterations to obtain a high purity individual rare earth oxides (REO) (Abreu and Morais, 2014).

Another problem associated with REY production is the handling of radioactive waste as most REY-rich primary magmatic deposits possess high concentrations of actinides; monazite contains 4-12 wt.% Th and although U concentrations are generally low, anomalous content of up to 14 wt.% can occur (Jordens et al., 2013). Uranium and thorium are both concentrated during the beneficiation of REY and the tailings wastes may exhibit high levels of radioactivity after cracking. Co-production of radioactive elements is feasible for the highest U-Th concentration ores, albeit with significant additional costs (Golev et al., 2014). These issues have led to notable pollution in China and Malaysia (Golev et al., 2014, Kolo *et al.*, 2015). For many sites, industrial processing is followed by costly remediation and waste disposal in long-term storage. Significant radioactive element concentrations constitute important economical drawbacks for any new REY exploitation project.

Considering the problems associated with magmatic-related REY deposits and despite their abundance, alternative sources of REE more readily beneficiated with low radioactive waste are attracting attention alongside efforts to increase recycling of REY from scrap or end-of-life consumer products. The abundance of neodymium-iron-boron magnets (NdFeB) in cell phones, hard drives and wind turbines forms the major target for this recycling effort with promising results on Nd recovery in the laboratory (Vander Hoogerstraete *et al.*, 2014). In addition, development of REY production from industrial waste or by-products such as red-mud (Ochsenkühn-Petropulu *et al.*, 1996, Tsakanika *et al.*, 2004, Qu and Lian, 2013, Liu and Naidu, 2014, Borra *et al.*, 2015, Deady *et al.*, 2016) and coal residue (Rozelle *et al.*, 2016a) has received considerable interest. These formations contain REY-bearing minerals and/or adsorbed REY that are transferred to the wastes during initial ore processing. These wastes constitute a low-grade resource with economically significant tonnage due to the importance and spread of the coal and aluminium industries (Goodenough *et al.*, 2016). Other alternative sources, include sea-floor deposits such as ferromanganese nodules (Fujimoto *et al.*, 2016), hydrogenetic crusts, and marine clays (Kato *et al.*, 2011, Menendez *et al.*, 2017) that can have significant REY concentrations (Hein *et al.*, 2013). Although of scientific interest, their relative inaccessibility and need for advanced mining technologies makes their economic exploitation challenging. As an initial approach to establish methods for REY-extraction from such marine formations, here we investigate sub-aerial equivalents of these deposits preserved in ophiolites; slices of ancient oceanic crust now present on-land that provide ease of access and sampling. Given that, the ferromanganese metalliferous sediments of the Troodos ophiolite in Cyprus known as umbers constitute an obvious best choice for study. These deposits represent direct analogue of actual oceanic metalliferous sediments formed in the vicinity of hydrothermal vents (Boyle and Robertson, 1984, Richards and Boyle, 1986, Boyle, 1990, Robertson and Varnavas, 1993a), and have been exploited since classical times for pigments. Nevertheless, to our knowledge no previous work has investigated the processing of these deposits as a potential source of REY.

This study investigates the potential recovery of REY from umbers, metalliferous sediments of the Troodos massif in Cyprus, as analogue to numerous oxide-based deposits found on-land that may provide an alternative to magmatic-related REY deposits that currently dominate global supply. Herein, we report the influence of various kinetic parameters such as the nature and concentration of lixiviant, reaction times, temperature and pulp density, on the release of REY during simple and sequential leaching experiments. We also explore in detail the efficiency of oxalate precipitation for the selective extraction of low concentration REY from other impurities present in the leach liquor via pH-dependent experiment and geochemical modelling.

2. Background geology

Umber deposits constitute the basal facies of the sedimentary sequence that accumulated above the extrusive lavas of the Troodos ophiolitic massif, Cyprus. These metalliferous formations resulted from the precipitation and accumulation on the paleo seafloor of Fe and Mn oxides from high temperature hydrothermal solutions in the Tethyan Ocean 91 million years ago (Robertson and Hudson, 1972, Boyle, 1990). Umbers are found interstratified with or overlying the Upper Pillow Lavas of the Troodos ophiolite as lenticular bodies or in shallow depressions of the lava surface. Although there are minor accumulations at multiple levels within the lavas, supra-lava umbers are by far the most abundant and these constitute the basal facies of the Perapedhi Formation, bracketed between the basaltic upper pillow lavas and radiolarian cherts of Campanian age (Robertson and Hudson, 1974). Massive umber deposits can reach thicknesses of 4 m, although most are limited to 1 m. However, records indicate that outcrops up to 35 m thick existed prior to extensive extraction in the Mangaleni quarry (Boyle, 1984) where production peaked at 6000 $t.y^{-1}$ (Morse and Stevens, 1979, Cyprus Geological Survey, 2006). The lateral extent of umber deposits is predominantly controlled by the initial sea floor topography, subsequent preservation from sea floor weathering and more recent anthropogenic activity since Classical to the modern era.

Umbers comprise brown Fe-Mn-rich mudstones with an amorphous oxyhydroxides-dominated mineralogy, formed by the accumulation of hydrothermal plume fall-out of Fe-Mn oxyhydroxides (Boyle, 1990). Umber deposits are commonly carbonate-free. Dissolved Fe and Mn from the effluent issued at hydrothermal vents oxidize in contact with bottom seawater to form colloids with strong surface charge that enables the efficient scavenging of dissolved species (Koschinsky and Halbach, 1995, Koschinsky and Hein, 2003). Umbers thus acquired seawater-like REE signatures with concentrations up to ~500 $mg.kg^{-1}$ total REY (0.06% total REO (TREO) as RE_2O_3) with low concentrations of radioactive elements (average U = 2.4 $mg.kg^{-1}$ and Th = 2.0 $mg.kg^{-1}$ (n=59) (Josso, 2017); Table 1).

Geochemical composition of supra-lava Umber (n=59)

SiO_2	17.5 ± 4.5	V	964 ± 220	Ce	41 ± 18
TiO_2	0.15 ± 0.05	Mo	38 ± 20	Pr	27 ± 12
Al_2O_3	3.7 ± 1.3	As	366 ± 84	Nd	103 ± 30
Fe_2O_3	52.1 ± 7.4	Zn	310 ± 54	Sm	22 ± 6
MnO	10.1 ± 2.6	Ba	1080 ± 553	Eu	5.7 ± 2.6
MgO	1.8 ± 0.5	Rb	21 ± 9	Gd	23 ± 6
CaO	1.7 ± 0.5	Sr	1038 ± 626	Tb	3.7 ± 2.4
K2O	0.6 ± 0.3	Y	98 ± 24	Dy	20 ± 5
P_2O_5	0.8 ± 0.3	Zr	90 ± 23	Ho	4.1 ± 1.3
Co	150 ± 37	Pb	179 ± 69	Er	10 ± 3
Ni	220 ± 57	U	2.4 ± 1	Tm	1.6 ± 1.2
Cu	736 ± 216	Th	2.0 ± 1	Yb	9.0 ± 2.1
Cr	20 ± 9	La	106 ± 29	Lu	1.3 ± 0.2

Major elements are expressed in wt.% ± 2 σ

Minor and trace elements are expressed in mg/kg ± 2 σ

Table 1: Typical geochemistry of unaltered supra-lava umbers from the Troodos massif [Josso, 2017].

These Fe-Mn oxide formations thus have similar concentrations to the ion-adsorption clay (IAC) deposits that are mined in southern China (ΣREY = 300 – 1500 $mg.kg^{-1}$, (Yang *et al.*, 2013)). By comparison with the most advanced rare earths projects in Europe, the REY content is 12 to 14 times lower than in the Khibina and Lovozero alkaline complexes of the Kola Peninsula and the Norra Kärr intrusion in Sweden, respectively 0.7% and 0.59% TREO (Chakhmouradian and Wall, 2012, Guyonnet et al., 2015). However, in contrast with these deposits, umbers possess an amorphous oxide dominated mineralogy and low concentrations of radioactive elements, and these may have advantages with regards to the overall extraction and treatment costs of the ore. Given the low content of targeted elements, it is of prime importance to identify the processing conditions that maximise the release of REY from umbers. We therefore explore the influence of major kinetic parameters of a variety of lixiviants used in the REY extractive industry, including acid and ionic solutions, on the recovery of REY to develop the best recipe for high extraction yields.

3. Material and method

3.1 Experimental leaching conditions and material

Leaching experiments were undertaken to investigate the potential recovery of REY from the metalliferous sediments. Leaching experiments tested a variety of common inorganic acids, such as nitric, sulphuric and hydrochloric acid, as well as ion exchange solutions of sodium chloride and ammonium sulphate, which are widely used in the treatment of IAC deposits in China (Yang et al., 2013). The experiments were designed to test the influence of solution concentration, liquid-to-solid (LS) ratios, time of reaction, and effect of temperature on the efficiency of REY extraction into

the liquid phase. Each factor was studied independently by keeping other parameters constant (Table 2).

		Tested parameter				Lixiviants	
		Molarity (mol/L)	**LS ratio**	**Time**	**Temperature**	**Ionic liquid**	**Acid**
Range	Min	0.05	2	2 min	20°C	NaCl	HNO_3
	Max	1.75	100	13 h	70°C	$(NH_4)_2SO_4$	H_2SO_4
When constant		1	25	120 min	20°C		HCl

Table 2: Range of experimental parameters and type of lixiviant used in the leaching experiments.

Batch reactions experiments were performed using 1 to 10 g of powdered samples mixed with the appropriate volume of lixiviant for the desired pulp density in closed 500 mL Erlenmeyer flasks. The kinetic influence of temperature on leaching efficiency was investigated at controlled temperature (40 and 70 °C) by mixing powdered samples and acid solutions (1 N HCl, HNO_3 and H_2SO_4) at 25:1 LS ratio for 2 h on a heating and stirring plate. The acid solutions were first placed on the hot plate for 1 h to thermally equilibrate prior to insertion in the flask.

Sample PJ-CY-2014-91 (Table 3), the primary focus for this study, was recovered south-west of Marki on the northeastern rim of the Troodos massif. It was chosen from a pool of other samples as representative of the mean umber composition (n = 59, (Josso, 2017)). The complete sample set and its geochemistry are presented elsewhere [Josso et al, in prep]. Sample PJ-CY-2014-91 is devoid of weathering or known alteration affecting some umbers such as silicification or diagenetic remineralisation that involves removal of Mn and formation of apatite enriched in REY. The sample was first crushed using a manual press and dried for 48 h at 65 °C. Once dried, the crushed material was milled in agate pestle and mortar. Quantitative grain size data of the powdered umber were obtained using a Malvern Mastersizer laser particle size analyser at the National Oceanography Centre Southampton (NOCS). Two aliquots of the sample were measured in triplicate with good reproducibility (Supplementary Table 1). After grinding, 90% of the sample size fraction is less than 370 μm in diameter, which constituted the working material for the following leaching experiments.

sample PJ-CY-2014-91					
SiO_2	24.1	Ni	308	Nd	110.1
TiO_2	0.2	Cu	801	Sm	22.5
Al_2O_3	6.0	Zn	314	Eu	5.6
Fe_2O_3	38.1	Ba	982	Gd	23.3
MnO	12.2	Sr	244	Tb	3.5
MgO	2.4	Zr	115	Dy	20.0
CaO	1.24	Th	4.6	Ho	3.9
K_2O	1.2	U	1.5	Er	10.3
Na_2O	0.7	Y	97.0	Tm	1.5
P_2O_5	0.5	La	122.5	Yb	9.0
Sc	11.6	Ce	66.3	Lu	1.3
Co	119	Pr	27.0	ΣREY	523.7

Table 3: Composition of sample PJ-CY-2014-91 used in leaching experiments. Major elements are expressed in wt.%, trace elements in mg/kg.

3.2 Oxalate precipitation

The precipitation of REY from a pregnant leach liquor was investigated by the addition of ammonium oxalate at various pH values. A stock leach solution (SLS) was first produced by the leaching of 20 g of umber by 600 mL of 1 N HCl over 2 h at laboratory temperature (~21 °C). This solution was used as a reference material for all further precipitation experiments and its composition after filtration of the solid residue through 0.45 µm cellulose nitrate membrane filters is presented in Table 4. For each precipitation experiment, 20 mL of the SLS was transferred into 50 mL Falcon tubes, to which was added 7 mL of a 0.32 N solution of ammonium oxalate $(NH_4)_2C_2O_4.H_2O$. The pH of each experiment was then immediately adjusted to the desired pH value (ranging between 0.85 and 3.15) by the addition of ammonia solution and measured with a Thermo Scientific Orion pH meter calibrated at laboratory temperature. All reagents used were at least analytical grade or higher purity. Solutions were left to rest for 5 h and a white precipitate was observed in all vials after this time. Tubes were then centrifuged and the liquid phase carefully transferred into pre-weighed HDPE bottles, whereas the precipitate was redigested with 6 N HCl and transferred to pre-weighed HDPE bottles. Both resulting solutions were analysed by ICP-MS for major elements, trace elements and REY. A mass balance was undertaken to check the measurement quality by ICP-MS and assess the experimental workflow. Our results normalized to the concentration in the stock leach solution show that the mass balance for cumulated solution and oxalate precipitate is good (90% - 110% of initial mass) for Na, Mg, Al, Ti, Mn, Fe, V, Co and Ba. Recovery for Ni, Cu, Sr, Y, Zr and REE ranges between 75 and 100% of the initial mass introduced depending on the element over the range of pH tested. In contrast, the masses of U and K were constantly found in higher proportions (110-120%) when compared with the initial mass introduced probably due to higher background noise and measurement precision on these elements. Calcium shows the greatest variations potentially linked to the formation of insoluble Ca oxalate phases during the preparation of daughter solutions with 3% nitric acid for ICP-MS analysis. Nevertheless, these data are of sufficient quality to determine the general phase distribution of each element during the precipitation of oxalates from the SLS at different pH values.

	Na	Mg	Al	K	Ca	Mn	Fe
SLS (n=3)	67.4	44.7	24.2	21.6	121.2	100.9	71.3
Abs. Std. Dev.	1	0.6	0.3	0.3	1.2	0.8	0.5

	Sc	Ti	V	Co	Ni	Cu	Sr	Y	Zr	Ba	Th	U
SLS (n=3)	39	684	3597	1105	548	1587	3537	2682	24	3099	32	23
Abs. Std. Dev.	0.3	4.5	9.5	2.2	3.4	2.2	7.8	4.2	0.2	2.9	0.1	0.1

	La	Ce	Pr	Nd	Sm	Eu	Gd	Tb	Dy	Ho	Er	Tm	Yb	Lu
SLS (n=3)	3651	653	826	3582	730	186	763	108	624	117	297	37	207	28
Abs. Std. Dev.	3.6	1.3	1.0	2.1	1.0	0.3	0.6	0.2	0.8	0.2	0.3	0.2	0.5	0.2

Major elements expressed in mg/L, trace elements in µg/L

Table 4: Composition of the stock leach solution (SLS) presented as the mean of triplicate and absolute standard deviation

3.3 Analytical procedure

Major, trace and rare earth elements concentrations were determined by inductively coupled plasma mass spectrometry (ICP-MS) using an Element X-series 2 at National Oceanography Centre Southampton (NOCS). Solutions for measurement by ICP-MS were diluted to appropriate total concentrations with a 3% nitric acid solution containing an internal spike with In-Re (5 $\mu g.kg^{-1}$) and Be (20 $\mu g.kg^{-1}$). Artificial element standards were produced at 2, 5, 10, 25, 50, 75, 100, 125, 150, 175 and 200 $\mu g.kg^{-1}$ and used together with the internal spikes to calibrate the instrument and monitor sample drift corrections. All standard calibration curves display less than 3.5% analytical error with excellent linearity. International rock standards BHVO2, BIR1 and JB3, were run in triplicate as unknown to monitor accuracy of calibration with excellent reproducibility between triplicates (Supplementary Table 2). All analysis for trace and rare earth elements, Mg, Al, Fe and Mn are accurate and fall within the range of published recommended values (Jochum *et al.*, 2005). Sodium was measured in excess by 6% and 3% in BHVO2 and BIR1 respectively, whereas Ca and Ti concentrations were 3% below recommended range in JB3. Measurement reproducibility on international standards was also checked for discrepancies between standards prepared with and without ammonium oxalates to check for matrix effects from the oxalates. Standard dilution to daughter solutions were prepared by including ammonium oxalate matching the final concentration of $(NH_4)_2C_2O_4$ in samples analysed by the ICP-MS. Excellent reproducibility of results, showing less than 5% difference between standards with and without oxalates, indicates the absence of any matrix effects.

3.4 Scanning electron microscopy imaging

Imaging of the oxalate precipitate was obtained by scanning electron microscopy (SEM) at University of Southampton using a Carl Zeiss LEO1450VP. The instrument used an operating voltage of 20 kV and a working distance of 19 mm. The AZtec Energy Software was used for the processing of energy dispersive X-ray spectroscopy (EDS) with a process time of 5 on an average of 3300 $counts.s^{-1}$. Images were collected using a nominal probe current of 800 pA. The leachate was treated with ammonium oxalates and the pH equilibrated with aqueous ammonia. The solution was filtered and the residue washed with deionized water and then deposited onto Al-Cu pellets. The samples were left to dry in an oven at 60°C overnight and C-coated prior to analysis.

3.5 Speciation modelling

A numerical modelling approach, reproducing the conditions of the precipitation experiment was developed to assess rare earth element fractionation results in the oxalate precipitate. Modelling calculations were performed using the hydrogeochemical code PHREEQC version 3.3.9 (Parkhurst

and Appelo, 2013) and the thermodynamic data for REE from the Lawrence Livermore National Laboratory (LLNL) database (Delany and Lundeen, 1990). The LLNL database was supplemented by stability constants for the following aqueous RE-oxalate complexes; $REHOx^{2+}$, $REOx^{+}$, $RE(Ox)_2^{-}$ from Schijf and Byrne (2001), where "RE" represents any lanthanide (except Pm) and "Ox" abbreviates the oxalate ion $C_2O_4^{2-}$. Presently there is no complete set of stability constants for solid RE-oxalate complexes ($RE_2Ox_3.nH_2O$). Missing constants were obtained via linear free-energy relationship (LFER) calculations using existing data on RE-oxalate binding (Chung *et al.*, 1998) compared with constants in the NIST database from other complexing agents (Smith and Martell, 2004). Best linear regression was obtained for a Phenol ($R^2 = 0.94$) and used for estimating constants absent in Chung et al. (1998) (Supplementary Figure 1).

4. Results

4.1 Leaching with ion exchange solutions

Leaching experiments using ammonium sulphate ($(NH_4)_2SO_4$) or sodium chloride (NaCl) at different concentrations (0.05 – 1.75 N) and at a LS ratio high enough for the electrolytes not to be considered a limiting reactant (up to 100:1) are not effective for the leaching of REY from umbers (Figure 1). These solutions generally target the most easily exchangeable cations but the maximum cumulated REY concentration in the leachate represents just 1.3% recovery of the initial REY content of the sample.

4.2 Leaching with acid solutions

Acid-promoted release of REY displays hyperbolic trends of recovery for all kinetic parameters tested (Figure 1). The experiments on acid concentration display curves approaching 80-85% recovery of the initial REY content in the acid leach after levelling off. A threshold concentration (before asymptotic values) is achieved for normality superior to 0.8 N H_2SO_4, HCl and 0.75 N HNO_3. Further increases of the normality improve the recovery of REE by only a few percent whereas contaminant concentrations continue to increase. REY recovery levels using HNO_3 are smaller compared with HCl and H_2SO_4. Although all three are strong acids, there are multiple orders of magnitude difference in their respective dissociation constant (pK_a = -6.3, -3 and -1.4 for HCl, H_2SO_4 and HNO_3 respectively) which explains the lower efficiency of HNO_3.

Another important factor influencing REY recovery is the Liquid-to-Solid (LS) ratio, or pulp density. REY yields increase with increasing LS ratio up to 20 with recovery rates of 72%, 83% and 82% for nitric, sulphuric and hydrochloric acid respectively. Further improvements in REY recovery is only minor at higher LS ratios for nitric and hydrochloric acid. In contrast, an improvement of nearly 10% is achieved with sulphuric acid between SL ratio of 20 and 100. This effect can be partly explained

by the partial neutralisation of the diluted acid during the reaction with umbers (Ochsenkühn-Petropulu et al., 1996).

A threshold reaction time greater than 100 min is observed for the two acids tested here with only minor improvements in REY recoveries for longer leaching times (Figure 1). For HCl, the total recovery increases for the first 2 hours of reaction then levels off, with only a 4% gain in the recovery of REY in the next 11 h of additional reaction time. The reason why the sulphuric acid gave lower yields compared to other tests at equivalent concentration, LS ratio and time of reaction is not known. Nevertheless, during reaction more than 75% of the total recovery was achieved after only 15 min for both acids, suggesting rapid reaction kinetics of extraction. However, the major elements recovery continuously increased with reaction time, therefore, shorter reaction times limit the amount of impurities mobilised into the leach liquor.

As acid activity increases with temperature, elemental recovery in the leach increases as a function of temperature. Recovery for REY increases by 19% when using HCl as the leaching temperature rises from 20 to 70 °C, ultimately reaching 93% recovery of the initial REY content. However, no improvement in REY recovery is observed when increasing the temperature for the nitric and sulphuric acid leach.

These results show that temperature is a key parameter during REY recovery using HCl especially at temperatures of around 70 °C.

In all experiments, the recovery of U and Th follow similar trends to the REY but reaching asymptotic recoveries between 20 and 50% for Th and 40 to 70% for U across the range of parameters tested. Despite the discernible mobilisation of these elements, their combined concentrations are below 3 $mg.kg^{-1}$ in all leachates.

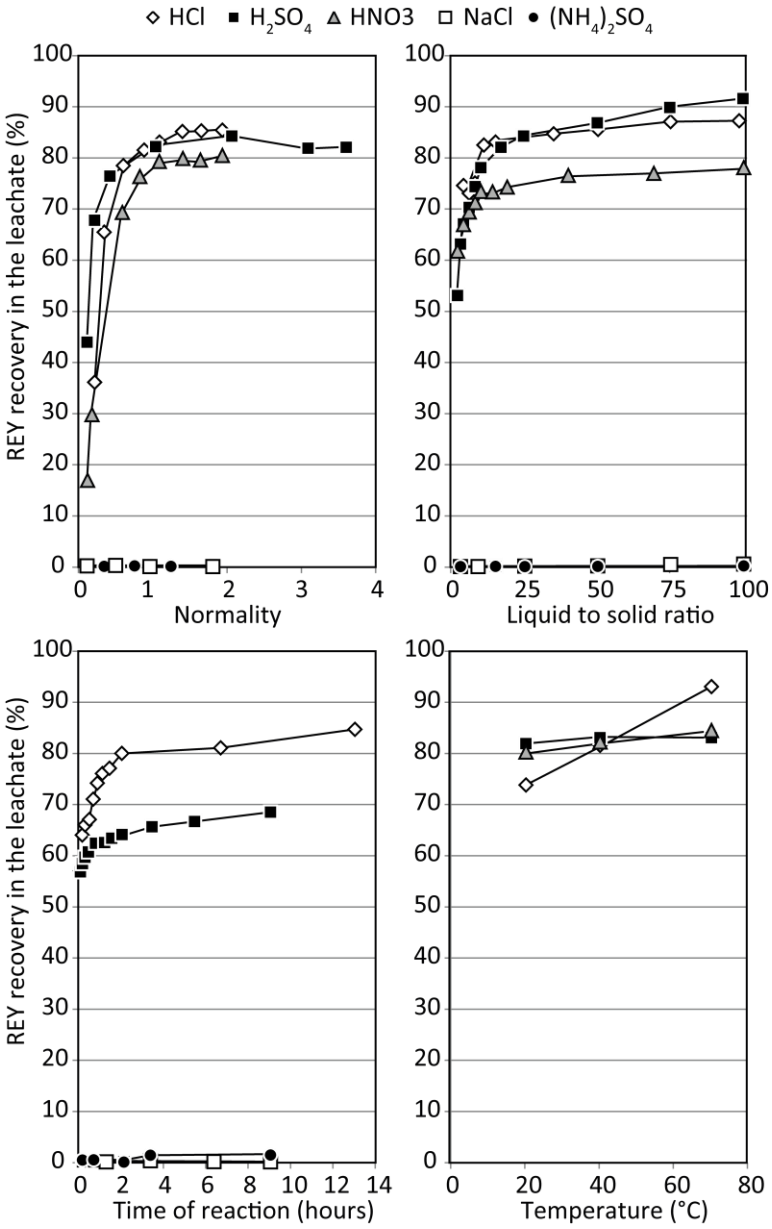

Figure 1: Rare earth element and yttrium recovery in the leaching solution testing the influence of lixiviant molarity, liquid to solid ratio, time of reaction and temperature.

4.3 Multiple stage leaching conditions

Simple leaching experiments recovered > 80% of the initial REY content of the sample with acid concentrations greater than 0.8 N. Unfortunately, undesirable impurities such as Ca and Na also display strong leaching efficiencies (40 – 70%) in the weakest acid concentrations.

A two-stage leaching process was designed using 0.05 N HCl acid for 1 h in a first stage (L1) to investigate the possible separation of impurities contained in easily dissolved phases from rare earth and yttrium. Following centrifuging and extraction of the liquid phase, a 1 N acid solution is introduced to the sample and allowed to react for another hour on a shaking table (L2).

The first leach with weak acid shows that 66% of Ca, 64% of Na and more than 20% of Sr and U passes into solution (Figure 2). The release of REY in L1 is moderate ranging from 12 to 21% although the most abundant RE, La and Nd, are amongst the least mobilized. In contrast, yttrium, third most abundant RE in umbers shows the greatest recovery of the RE during the first stage of leaching (~21%). In L2, the REY recovery is greater than 65% (up to 76%, with the exception of Ce) for the 3 most abundant REY (La, Nd, Y) whereas the recovery continuously decreases for the heavy REE (HREE) with only 43% recovery for Lu. Similar trends and levels of recovery were observed for L1 with other weak nitric acid leaching whereas L2 is closer to HNO_3 and HCl recovery trends at higher molarity although yields are lower by 10 to 20% (supplementary Figure 2).

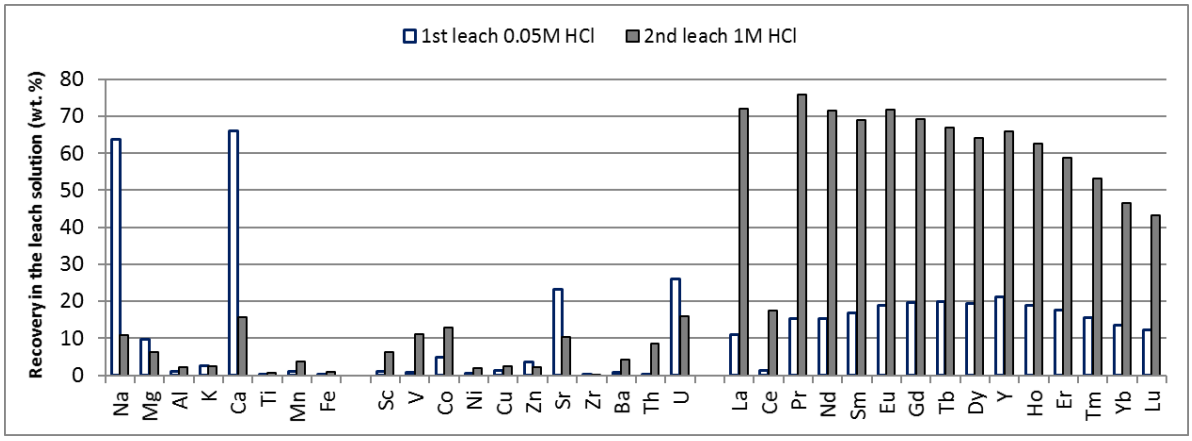

Figure 2: Two step leaching experiment on sample PJ-CY-91.

Consequently, a two-stage leaching process appears to be a viable way of increasing the purity of the leach solution containing the dominant fraction of REY by removing 60 - 65% of the main impurities Ca and Na. These elements are present at less than 15% of their initial concentration in L2 compared to a single leaching step. However, 13.5% of the sample's REY, equivalent to 19.6% of the overall inventory of leachable REY, are lost at the L1 stage, which constitutes an important loss considering the already low concentrations of REY in the umber ores available for recovery. Although the leaching efficiency for most major elements is below 10% (apart Na and Ca), the mass of major elements dominate the overall composition of the leachates and highlights that further steps of purification are needed.

Protocols of sequential leaching for nodules and hydrogenetic ferromanganese crusts (Koschinsky and Halbach, 1995) have already been widely used for the study of trace elements partitioning between the main mineralogical phases of these marine deposits. Applying this protocol to umbers yielded no significant REY recoveries for the first 2 leachates using acetic acid and hydroxylamine hydrochloride (5.8% and 3.9% respectively). Most REY were retrieved in the solution during the third leach when oxalic acid is employed attacking the dominant amorphous Fe oxide fraction of umbers. However, although REY recovery was good (53%), impurities, mainly Fe, were far greater

than in other leachates previously produced, and the oxalic acid protocol is considered too aggressive for the purpose of this study.

4.4 Purification of the leachate via oxalate precipitation

The precipitation of REY as an oxalate cake is widely used in industry for the selective extraction of targeted metals (Vander Hoogerstraete et al., 2014, Xie et al., 2014). However, this method is usually applied to leachates of pre-concentrated REY-bearing minerals such as xenotime, bastnäsite or monazite (Xie et al., 2014). These approaches form REY-rich leachates (1 to 40 $g.L^{-1}$) and limit the amount of impurities in the solution. In contrast to leach solutions produced by the treatment of pre-concentrated REE-bearing minerals, the challenge of this study lies in the initially low rare earth elements concentration of the leach (0.1 - 0.5 $g.L^{-1}$) and the high concentration of impurities imposed by the non-pre-treatment of umbers for the concentration of a REE-bearing phase. We investigated, as a function of pH, the selective precipitation of RE-oxalate from other elements considered as impurities.

4.5 Elemental partitioning between solution and precipitate in various pH

The distribution of measured element concentrations between the initial leachate and subsequent precipitate is calculated as a mass percentage (Figure 3). Over the range of pH values considered, Na, Mg, Al, K, Ti and Fe do not appear to partition into the solid phase, with less than 1% of the measured mass retrieved in the precipitate for Mg, Al, K and Fe, and < 2% for Na and Ti. Ca shows the greatest variation with no precipitation at pH < 1.2 and nearly complete precipitation achieved with the oxalate at pH > 1.5. The virtually complete precipitation of Ca observed in the pH window 1.2 - 1.5 appears to drive most of the other major element variations (Figure 3). Manganese precipitation begins at pH = 1.5 and gradually increases from 0.3% at pH = 1.5, to 8.6% at pH = 3.15. Similar precipitation trends are observed for Ba and Sr that are completely depleted in the precipitate at pH < 1.5, and then strongly and continuously increase as pH becomes less acidic, with up to 45% and 89% mass fraction in the solid for Ba and Sr respectively at pH = 3.15. Scandium, V, Co, Ni, Cu display a similar behaviour with important precipitation occurring at pH = 1.5, although their relative fraction in the solid phase decreases at higher pH values. These patterns (Figure 3) suggest metal co-precipitation with Ca oxalates, the dominant phase of complexation by mass.

The partition trends of the REY into the solid show that nearly complete precipitation of rare earth elements with oxalates is achieved between pH 1.3 and 2.3 (Figure 3). Outside of these limits, the fractionation varies along the REE series. In the pH window 0.75 - 1.3, all REY show increasing affinity for oxalate complexes as a function of increasing pH. However, this fractionation between the solid or liquid phase is not equal across the lanthanides. Uptake within the solid phase increases from La to Eu to then decreases until Lu. In contrast, at pH > 2.5 a decreasing gradient of affinity for

the oxalate ligand is observed from light to heavy REE, which suggests a control of the ionic radius on the complexation of REE with oxalates at pH > 2.3 where light REE are preferentially incorporated over HREE.

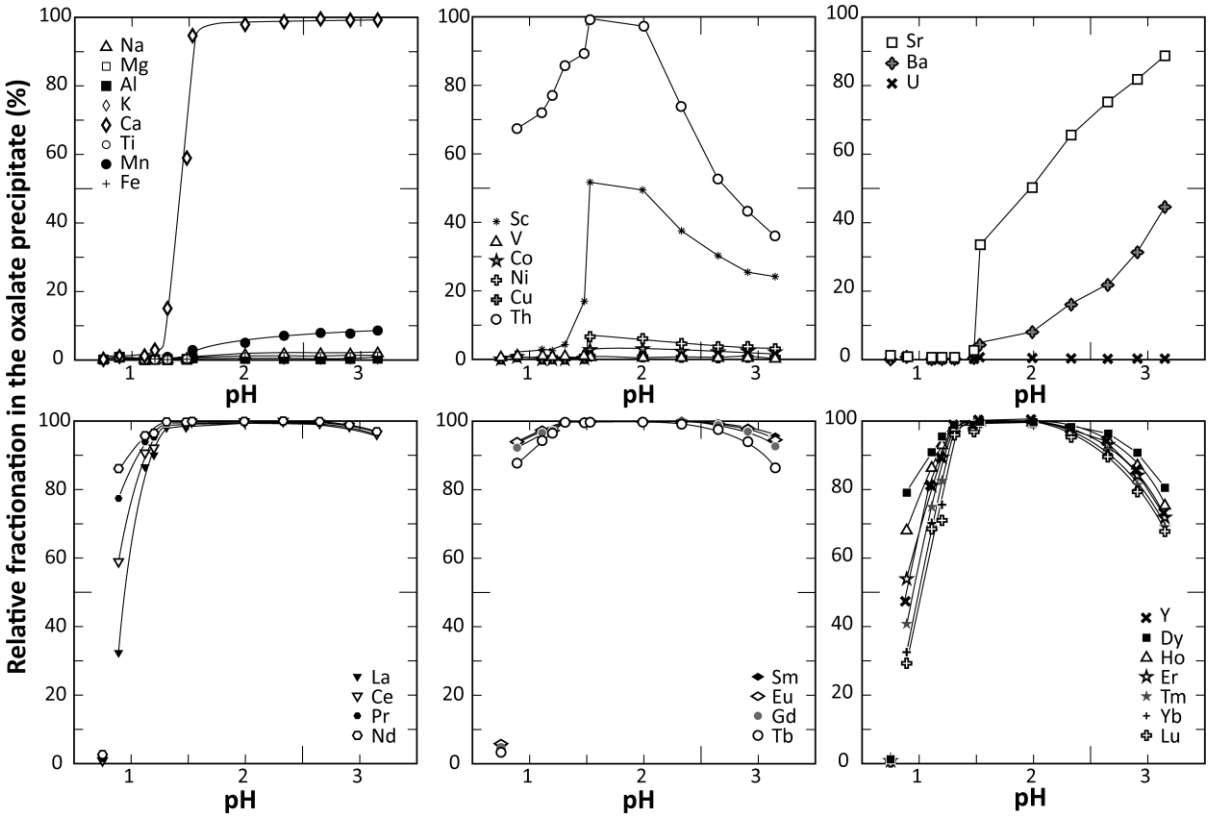

Figure 3: Element fractionation in the oxalate precipitate (mass percentage) as a function of pH from the stock leach solution.

4.6 Purity of the precipitate

As demonstrated by the mass distribution between solid and liquid phases, the precipitation of oxalates constitutes an effective stage for the purification of the leach solution. Nearly complete precipitation of REE can be realized, while most major and trace elements, considered as impurities, remain in solution. However, these trends do not address the purity of the precipitate, as substantial differences in mass are not considered in the above results.

The purity of the precipitate is analysed as the ratio of the total mass of rare earth and yttrium (REY) divided by the sum of all measured masses (Figure 4). Disregarding the mass of the oxalates, the total mass of the precipitate expressed as the sum of all other elements measured in the oxalate precipitate range from 30 to 4900 µg with Ca making up 70 to 91% of the precipitate at pH > 1.3. Accordingly, with more than 90% of the total REY mass precipitated from the stock leach solution at pH > 1.1, the purity increases strongly at lower pH, where mostly REY bind with oxalates to reach a maximum at pH 1.1. The purity then decreases as Ca, the main impurity, starts to precipitate. The cumulated masses for all other elements apart from Ca and REY only account for 18 wt.% of the

precipitate at pH = 1.1 and less than 10 wt.% above pH 1.3, and is dominated by Mn, Cu, Ni, Na, and Fe.

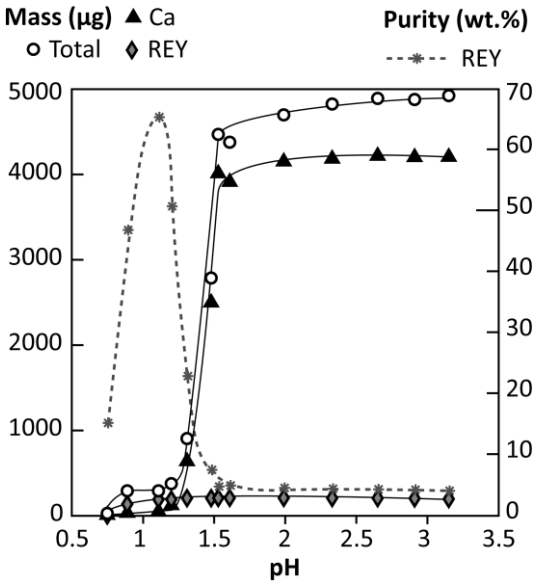

Figure 4: Element masses within the oxalate precipitate as a function of pH. The right-hand axis represents the REY fraction or purity of the precipitate (%).

4.7 Precipitate structures

Duplicates of the oxalate precipitation experiments were completed at pH 1.1 and 2.5 for SEM imaging. Two distinct crystal structures are observed between the two experiments, which reflects the difference in composition, notably the Ca content. At pH 1.1, oxalate crystals show platy prismatic and rectangular shapes up to 100 µm with smaller crest-like crystals covering them (Figure 5 A and B). Studies of $Ln_2(C_2O_4).nH_2O$ crystal microstructure (Zinin and Bushuev, 2014) have demonstrated crystallization of RE-oxalate in the monoclinic system. Oxalate crystals formed at pH 2.5 consist predominantly of small (~10 µm) rhombic bipyramid (Figure 5 C & D). Energy-dispersive X-ray spectroscopy (EDS) data were acquired for bulk areas, zones with specific crystal structure as well as spot analyses. The EDS spectrum and associated chemical data (Figure 6, supplementary table 3 and 4) are in good agreement with previous results on the purity of precipitates deduced from ICP measurements.

The EDS spectra highlight that 9 out of the 15 REY are in detectable range within the oxalate crystal at pH 1.1 whereas only Y, La and Nd, the three most concentrated REY in the experiment are detected in oxalate crystals precipitated at pH 2.5 (Figure 6). The total REY content at pH 1.1 is estimated to represent 85 to 94% of element precipitating with the oxalate. Variations of composition and REY distribution between the different crystals morphologies do not appear to correlate with shape or size. Large and well-formed crystals analysed (area_Xlarge and area_Xlarge2) encompass the range of measured REY concentrations, whereas smaller crystals with

a crest-like shape have an intermediate composition (Supplementary Table 3 and 4). At pH 2.5, Ca dominates the elements co-precipitating with oxalates (78 – 85%) and combined Y, La and Nd concentration reach a maximum of 7%, in good agreement with ICP-MS results and purity estimates (Supplementary table 3 and 4).

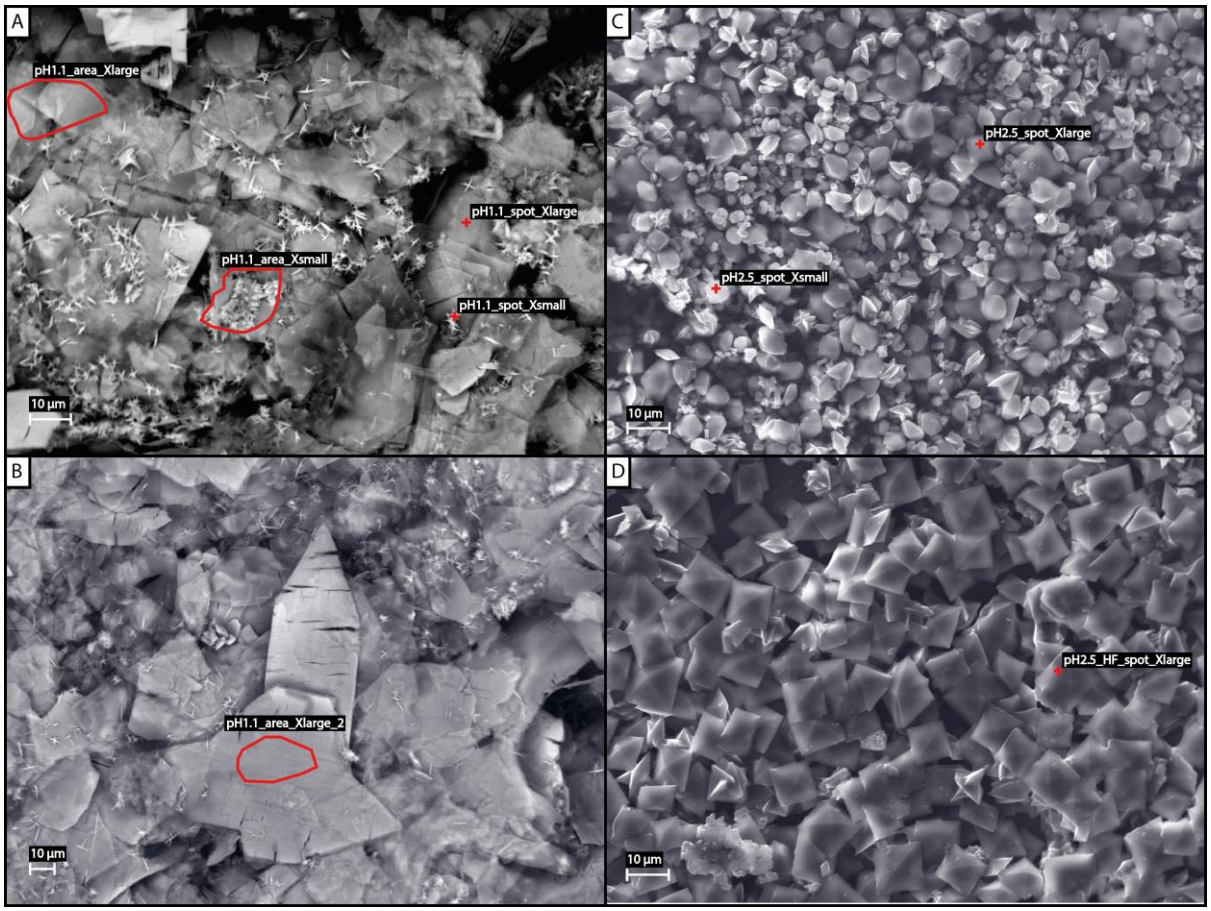

Figure 5: Backscatter image of oxalate precipitate at pH 1.1 (A and B) and at pH 2.5 (C and D). Areas and location of EDS spot analysis are shown on the figure (Supplementary tables 3 and 4).

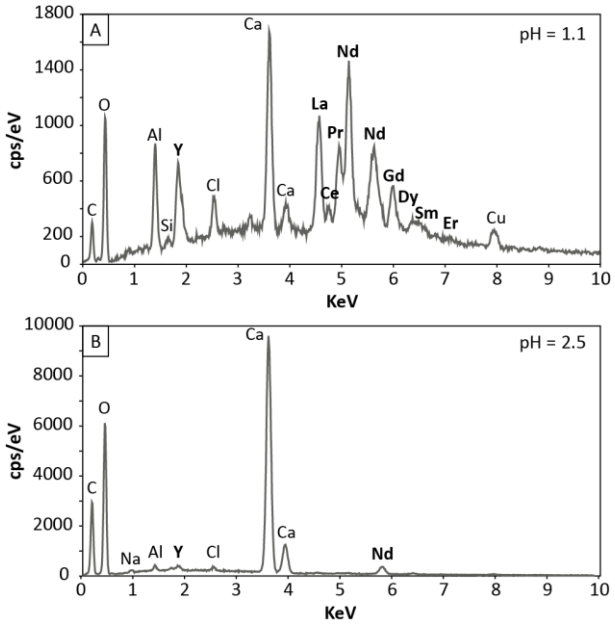

Figure 6: EDS spectrum of the oxalate precipitate obtain at pH 1.1 (A) and 2.5 (B). The spectra correspond to the field of view in images A and C of Figure 5. The presence of Al and Cu in measurement (A) reflects the composition of the Al-Cu pellets, these elements are absent of any precise crystal EDS analysis otherwise.

4.8 Overall REY recovery and distribution

The stock leach solution used for the oxalate precipitation experiment, corrected for appropriate dilution factors regarding sample PJ-CY-2014-91, contain 406 $mg.kg^{-1}$ REY consisting of 25.2% La, 24.7% Nd and 18.5% Y. The recovery rate for individual rare earth elements by the leaching procedure is > 95% for Pr, Nd, Sm, Eu, Gd, Y and Tb, 90% for La, with the recovery of the heavy rare earth elements decreasing with increasing atomic number from Dy (92%) to Lu (65%) (Supplementary Figure 3). The total REY content of the leachate consequently represents a yield of 77% of the initial REY content of the umber sample. The greatest loss occurs due to the poor recovery of Ce (30%), which contributes up to 62% of the total REY content not mobilised by leaching. In contrast to the other trivalent REE, Ce is present as Ce^{4+}, which forms acid-resistant Ce oxide complexes (Bau and Koschinsky, 2009).

The formation of an oxalate precipitate has been demonstrated to be an efficient way of selectively precipitating REE from the solution and separating them from other impurities with an efficiency strongly dependent on pH. The minimal uptake during precipitation is observed for pH = 0.89 (61.5%) and rapidly increases up to pH = 1.3 where precipitation efficiency is > 96% for all REY. Adding the efficiency of oxalate precipitation on the leaching process (85% recovery at 70 °C), the REY recovery in the oxalate precipitate relative to the original sample increases from 51% of the initial REY content at pH = 0.89 to 82% for pH = 1.3 – 2. Relative to the impurities that are co-precipitating, the optimal purity for the precipitate is achieved for pH = 1.1 where 76% of the initial REY content of the sample is recovered. Based on these values following optimal leaching and precipitation conditions, the processing of 1 ton of umber with an average 500 $mg.kg^{-1}$ REY would produce an oxalate precipitate containing 380 g of mixed rare earth elements.

4.9 geochemical modelling of REY recovery

4.9.1 Model conditions and available data

Detailed recovery trends within the oxalate precipitate (Figure 3) have highlighted the strong fractionation that occurs along the lanthanide series at pH values < 1.5. In addition, the decreasing recovery observed at pH > 2 as a function of atomic number constitutes another unexplained observation. Although HREE are present in only minor concentrations in umbers (average ∑HREE = ∑[Tb-Lu; Y] = 147 ± 34 $mg.kg^{-1}$, n = 59, (Josso, 2017)), they attract the greatest commercial values, which justifies further exploration of the reasons for their less efficient recovery. Furthermore,

speciation of oxalic acid as a function of pH (Supplementary Figure 4) shows that the presence of oxalate ion $C_2O_4^{2-}$ is minimal in the pH window considered here, although the precipitation of REE oxalate is observed at pH 0.8 and decreases at higher pH when the activity of Ox^{2-} increases (Supplementary Figure 4 (Chi and Xu, 1998)). To explore these questions, speciation modelling was performed using PHREEQC (Parkhurst and Appelo, 2013) to reproduce the chemistry involved in the precipitation experiments.

Following the conditions of the precipitation experiments, the REE contained in the leachate are partitioned between the solution and the precipitate formed after the addition of ammonium oxalate. However, not all oxalate ions will be in the correct ionic form to bind with REY to precipitate and form aqueous complexes that may remain in solution (supplementary Figure 4). Potential aqueous complexes of REY^{3+} and oxalates can be described (Eq. 1 and 2) taking into account the bioxalate (HOx^-) and oxalate (Ox^{2-}) ions such that:

Eq. 1: $$_{HOx}\beta_m = [REY(HOx)_m^{3-m}]$$

Eq.2: $$_{Ox}\beta_n = [MOx_n^{3-2n}]$$

Where $_{HOx}\beta_m$ is the m^{th} (order of complexation) stability constant of the bioxalate (HOx^-) ion with any REY^{3+} and $_{Ox}\beta_n$ the n^{th} stability constant of oxalate ion (Ox^{2-}) with any REY^{3+}. Schijf and Byrne (2001) showed that one orders of complexation for bioxalate (m = 1) and 2 for oxalate ions (n = 2) are satisfactory for modelling REY binding behaviour with oxalates in aqueous solution as further orders of complexation are minor.

Precipitating REE-oxalate complexes have been reported to form hydrated REY salts (Eq. 3) such that:

Eq. 3: $2REY^{3+} + 3OX^{2-} + nH2O \rightarrow REY_2Ox_3.nH_2O$

Although the formation of solid REY oxalates complexes has been considered since the 1950's (Crouthamel and Martin, 1951, Feibush *et al.*, 1958, Bhat and Rao, 1964, Grenthe *et al.*, 1969, Chi and Xu, 1998, Chung et al., 1998, Schijf and Byrne, 2001, Xiong, 2011), a complete set of solubility constants for solid rare earth oxalate remains elusive with no study presenting results for all lanthanides and Y simultaneously under identical experimental conditions. The most complete data set on $REY_2Ox_3.nH_2O$ complexes are from Bhat and Rao (1964), Chung et al. (1998) and Xiong (2011) (Table 5). Although diverging by two log units, two of the sets are consistent in showing increasing solubility constants from La to Gd, with decreasing values along the HREE. This behaviour contrasts with the variations in log $_{Ox}\beta_{1-2}$ for aqueous REY oxalates complexes that show a continuous increase across the lanthanides (Table 5).

Although data from Xiong (2011) lack information on HREE, they present a better comparison with those of Chung et al. (1998) with similar constants for La, Ce and Sm, whereas data from Bhat and Rao (1964) for La, Nd and Tb are low compared to their direct neighbours suggesting the presence of potential errors.

With relatively complete data over the lanthanide series and consistency with other studies, data from Chung et al. (1998) are used to estimate missing constants by using linear free-energy relationships in combination with the NIST databases for critical stability constant (Smith and Martell, 2004). Best matches were obtained by initially filtering the NIST database by $\log\beta_{La}/\log\beta_{Sm} < 1$ and $\log\beta_{Gd}/\log\beta_{Yb} > 1$ ratios to match the incomplete convex upwards trends formed by oxalate data. Accordingly, REE stability constants of 14 acids have been compared with data from Chung et al. (1998) (Supplementary Figure 1) and best-fit ($R^2 = 0.94$) observed for a phenol (2-Nitroso-1-Naphtol-8-sulfonic acid) giving the following equation of linear regression to estimate missing constant for Pr, Tb, Ho, Tm and Yb (Table 5), here exemplified for Pr (Eq. 4):

Eq. 4: $\text{Log}_{Ox}\beta_{Pr2Ox3.nH2O} = -2.232\ \text{Log}_{PHENOL}\beta_{Pr} - 18.88.$

	$\text{Log}_{HOx}\beta_1$	$\text{Log}_{Ox}\beta_1$	$\text{Log}_{Ox}\beta_2$	$\text{Log}_{Ox}\beta_{RE2Ox3.nH2O}$			$\text{Log}_{PHENOL}\beta$	Calculated $\text{Log}_{Ox}\beta_{RE2Ox3.nH2O}$	
	Schijf and Byrne (2001)			Bhat and Rao (1964)	Chung et al, (1998)	Xiong (2011)	Martell and Smith (1982)	LFER linear regression	% diff
Y	2.08	6.66	11.27	-28.91	-29.29	na	na	na	
La	1.92	5.87	10.47	-26.91	-29.22	-29.15	4.70	-29.37	-0.51
Ce	2.43	5.97	10.86	-28.79	-30.40	-30.18	5.04	-30.13	0.88
Pr	2.09	6.25	10.82	-29.64	na	-30.91	5.28	-30.67	
Nd	2.16	6.31	10.82	-29.69	-30.89	-31.57	5.46	-31.07	-0.59
Sm	2.35	6.43	11.08	-30.30	-31.35	-31.59	5.65	-31.49	-0.46
Eu	2.21	6.52	11.09	na	-31.38	na	5.61	-31.40	-0.08
Gd	2.04	6.53	11.10	-29.49	-31.37	-32.31	5.50	-31.16	0.69
Tb	2.29	6.63	11.27	-29.14	na	na	5.33	-30.78	
Dy	1.96	6.74	11.35	-29.44	-30.70	na	5.21	-30.51	0.62
Ho	2.17	6.77	11.41	na	na	na	5.10	-30.26	
Er	2.09	6.83	11.51	-28.82	-30.05	na	5.01	-30.06	-0.06
Tm	2.18	6.89	11.65	na	na	na	4.97	-29.97	
Yb	2.41	6.95	11.75	-28.25	-30.02	na	5.06	-30.17	-0.51
Lu	2.28	6.96	11.77	na	na	na	5.06	-30.17	

Table 5: Data used in the model to calculate REE speciation between aqueous and precipitating oxalate complexes. Missing data for solid oxalate complexes were calculated using LFER. Estimations between the linear regression and available data show at most ± 0.9% difference with published values.

The PHREEQC speciation modelling therefore considers the following reactions (Eq. 5 – 8) in addition to any form of complexation already included within the thermodynamic LLNL database used calculations:

Eq. 5: $RE^{3+} + HOx^{-} = REHOx^{2+}$ (aq.)

Eq. 6: $RE^{3+} + Ox^{2-} = REOx^{+}$ (aq.)

Eq. 7: $RE^{3+} + 2Ox^{2-} = RE(Ox)_2^-$ (aq.)

Eq. 8: $2RE^{3+} + 3Ox^{2-} + nH_2O = RE_2Ox_3.nH_2O$ (s)

In a similar way to REE, only partial data exists to describe oxalate complexation with other major or trace elements. Some data exists for Ca oxalates complexes (Martell and Smith, 1977, 1982), which is convenient for this study as Ca constitutes the dominant impurity in the REY liquor. Therefore, only the complexation of Ca and the rare earths are taken into account in this simplified model of previous experiments. The model was set up to calculate speciation of each rare earth with the 3 aqueous oxalate complexes and include the kinetic effect of REY-oxalate solid precipitation if saturation was reached.

4.9.2 Model results.

The 5 most abundant complexes present in the results of the model have been selected and are displayed on Figure 7. Combined they account for > 94% of REY complexes at the lowest pH and > 99% at pH > 1. Using experimental conditions and complexes calculated from the LLNL database, oxalate-binding dominates REE complexation. Other complexes considered in the calculation such as RE^{3+} and $REOH^{2+}$ are only present in the model at pH < 1 and account for less than 1% of dissolved REE.

Speciation calculated using PHREEQC with REE concentrations similar to those in the precipitation experiments displays important differences along the lanthanide series and show divergences with experimental results. In the range of pH and concentrations explored here, the Ca-oxalate complexes considered never reach saturation and remain in solution. In contrast with the experiments, no steep precipitation curve is observed between pH 1.1 and 1.5. Another major difference in the results from the model concerns the total lack of precipitation for Tb, Ho, Er, Tm, Yb and Lu. For these elements, complexation is dominated by aqueous single oxalates at pH < 0.8 and then by increasing proportions of double oxalate at more than 90% at pH > 1.6. It is important to note that these 6 elements have some of the lowest concentrations in solution ([RE] < 220 ppb). Interestingly, Eu precipitates although its concentration is only 138 ppb. All elements precipitating display convex upward trends of precipitation as a function of pH with a maximum reached for pH 0.9 - 1.1 (Figure 7). All these bell-shape curves show diverse degrees of slope inversely related to the concentration of RE in the stock leach solution. These observations suggest a control of both concentration and atomic number in the speciation of REE-oxalates.

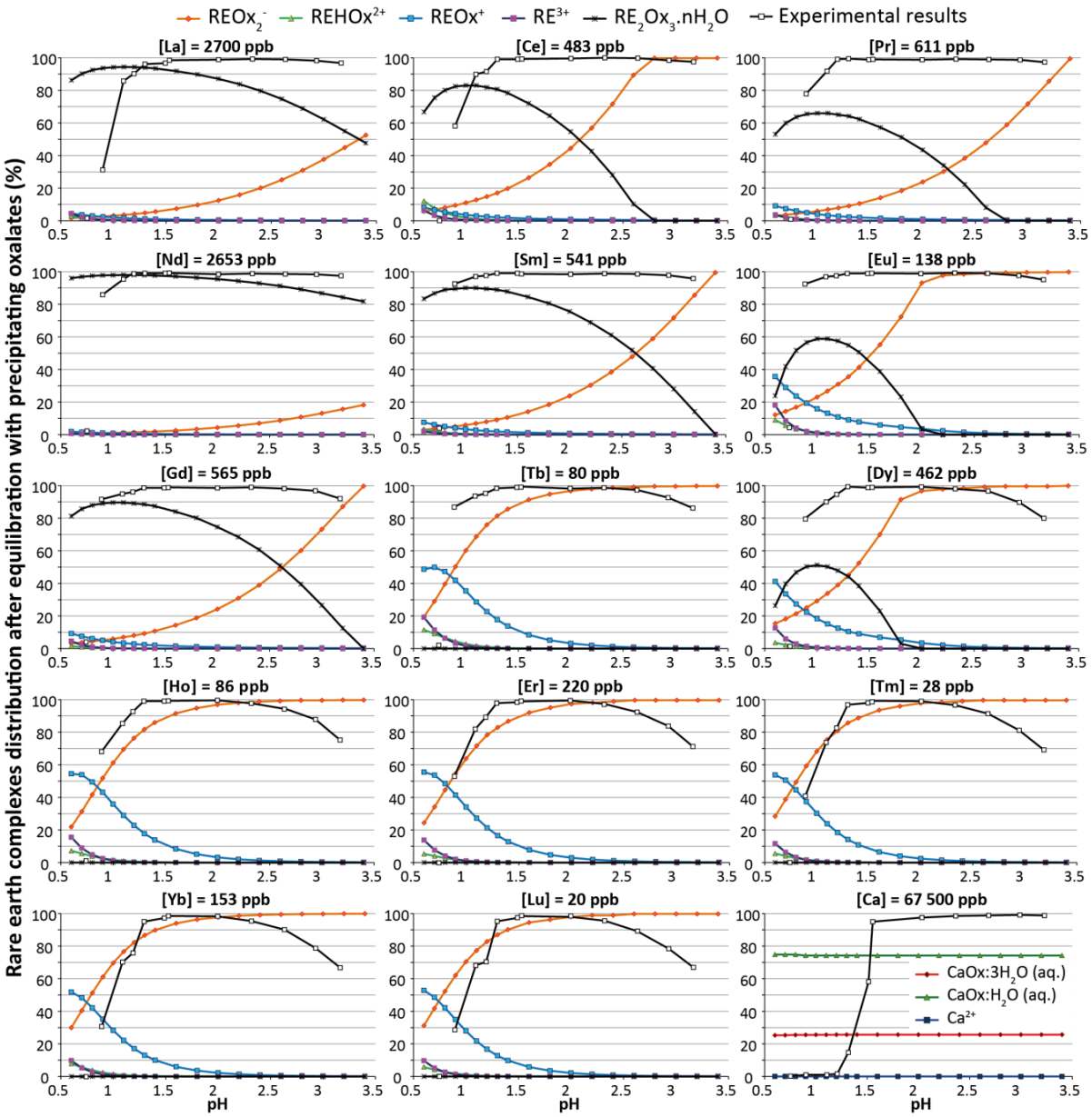

Figure 7: REE and Ca speciation with oxalate as a function of pH calculated using PHREEQC. Initial concentrations used replicate the initial experimental design. Experimental results (black line and white squares) are overlaid for comparison and should be compared with the modelling of $RE_2Ox_3.nH_2O$ complexes.

Accordingly, the modelling was further adjusted to test these hypotheses by calculating the speciation of all lanthanides in equal concentration at 0.1, 0.5, 1, 5 and 10 $mg.kg^{-1}$. Complete speciation results for each concentration are available in supplementary Figure 5 to 9. Figure 8 presents the formation of RE-oxalates precipitated at different concentrations for 6 selected rare earth elements along the lanthanide series. From the following models, the formation of solid RE-oxalate increases up to pH 0.9 - 1.1 but decreases thereafter. The position of the maximum precipitation is not constant and evolves from pH 1.1 to 0.9 as a function of increasing atomic number. In addition, the formation of a precipitate is directly affected by the initial rare earth concentration in solution. It appears that the formation of middle rare earth oxalate is favoured against light- and even more so against heavy-rare earth oxalate at equal concentrations. This

distribution can be considered as a direct representation of the stability constant $_{RE2Ox3.nH2O}\beta$ where constants increase from La to Gd and decrease again through the heavy rare earth elements. However, although the stability constant of La is the lowest, modelling shows formation of La-oxalate at potentially lower concentrations than is possible for the heavy rare earths to form solid complexes. This suggests that the HREE are affected by another parameter that inhibits their precipitation. Species distribution (supplementary Figure 5 to 9) highlights the increasing dominance of $REOx_2^-$ aqueous complexes as pH increase up to the point of inhibiting the formation of solid oxalates. Although the stability constant $_{Ox}\beta_2$ increases as a function of the atomic number (log K_2 = 10.5 - 11.7 from La to Lu) and could account for the decreasing formation in solid oxalates for HREE by competing in REE binding, this interpretation is counter intuitive considering $_{RE2Ox3.nH2O}\beta >> _{Ox}\beta_2$.

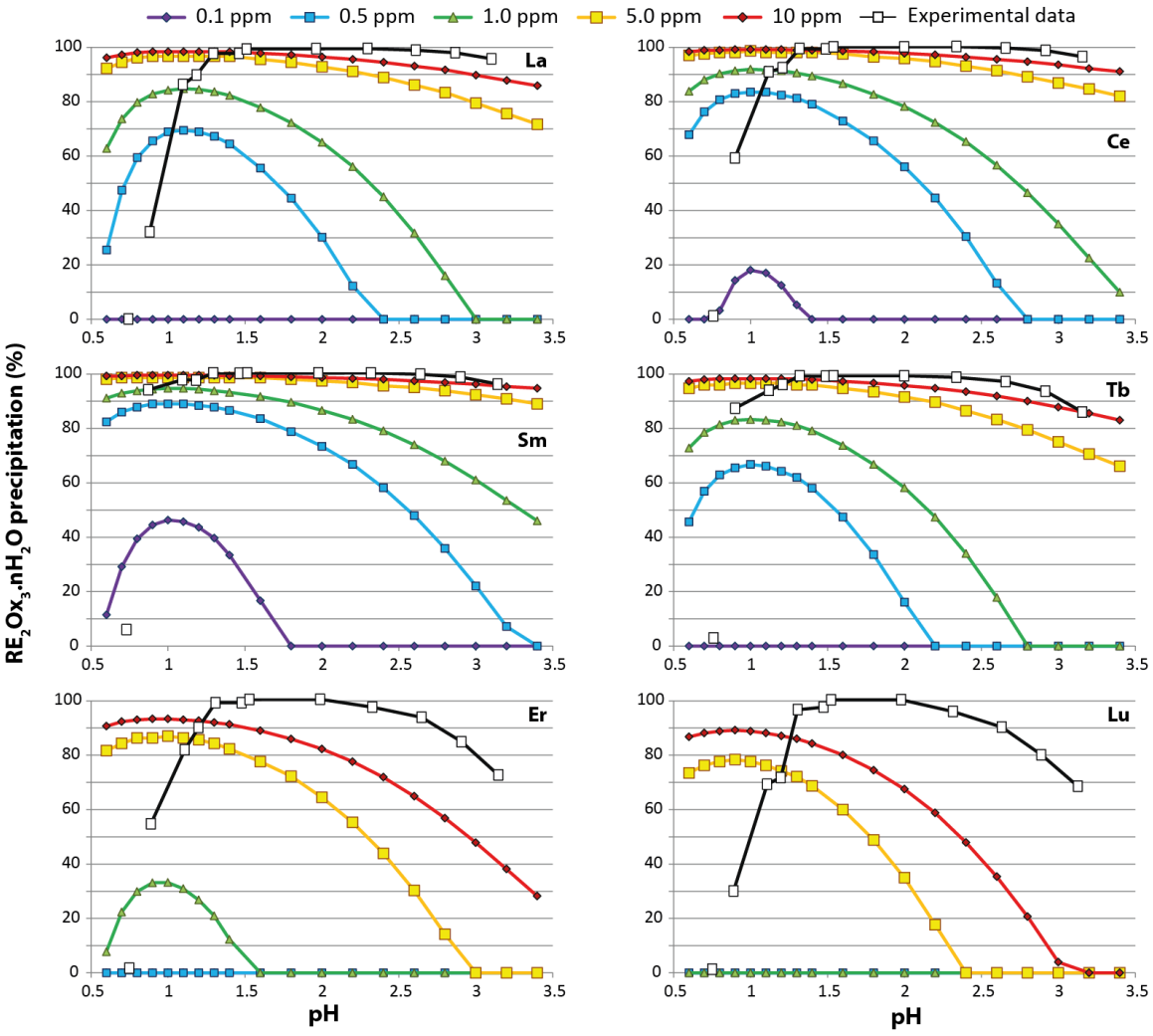

Figure 8: RE-oxalate precipitation as a function of the initial concentration of REE in the initial solution and modelling as function of increasing REE concentration. All other parameters are as in the experiment. Experimental results (black line and white squares) are overlaid for comparison.

Although the modelled and experimental trend for the precipitation of REE oxalate do not agree exactly, the model reproduces some of the observations from the experiments. For example:

1) The fractionation observed in the recovery from the experiments and the model at pH < 1.1 follows closely the bell-shape of the $RE_2Ox_3.nH_2O$ stability constant
2) The models show that at equal concentrations, the formation of precipitating RE-oxalate is favoured in the following order: MREE > LREE >> HREE. This trend results from (i) the positive gradient of $\log {}_{Ox}\beta_2$ along the lanthanide series coupled to (ii) the increase of competing species (e.g., dominantly Ca) consuming oxalate ions. Accounting for the initial differences in concentration in the experiment, this explains the decreasing recovery of the HREE observed in the experiment at pH > 2.

Under the model conditions, the maximum formation of a REE oxalate precipitate occurs at pH 1, similar to values previously reported for the purification of monazite leach liquor (Salman *et al.*, 2014). The species distribution following oxalic acid dissociation (Supplementary Figure 4) shows that Ox^{2-} ions represent less than 0.03% of the total oxalate species distribution at pH 1. In contrast, at pH 3 and above the Ox^{2-} concentration increases steeply and dominates species distribution at pH > 4.2. However, precipitation in the model is low. The dominance of Re_2Ox_3 complexes over aqueous complexes at pH 0.9 - 1.1 can be understood as a constant balance of the system. Free trivalent REE partitioning between the different oxalate complexes follows the magnitude of the stability constants. Therefore RE^{3+} will bind dominantly with Ox^{2-} over HOx^- to form a precipitate until Ox^{2-} becomes the limiting reactant. The system therefore balances the equilibrium induced by the decrease of $[Ox^{2-}]$ at a fixed pH, by dissociating more oxalic acid into HOx^- and Ox^{2-}. The newly formed Ox^{2-} ions are therefore readily available for complexation with free RE^{3+} in the solution and precipitate. The cycle carries on balancing until one of the other reactants becomes limiting. The decrease in Re_2Ox_3 at higher pH in favour of aqueous RE-oxalate complexes relates to the increasing competition in oxalate binding from Ca^{2+} which starts to precipitate at pH > 1.1 and is largely in excess over $[HOx^-]$ and $[Ox^{2-}]$. As pH rises, more oxalate and bioxalate ions bind with Ca over REY due to its much greater abundance in solution; 25 to > 3000 times the REY concentration. Oxalates constitute a chelating agent for REE and usually binds forming bidentate ligand with a ring structure to form precipitates (Hansson, 1970, Rao *et al.*, 2004). The decreasing availability of Ox^{2-} at higher pH due to binding with Ca, prevents the formation of these ring structure and explains the dominant complexation of RE^{3+} as aqueous complexes.

The absence of Ca oxalate precipitation in the model may explain the observed difference between REY recovery trends from the model and the experiment at pH > 2. In the experiments, Ca oxalate is the dominant precipitate at pH > 1.5 and REY are included as co-precipitating elements within the newly formed crystals. This may explain why REY recovery trends do not decrease as steeply as in the numerical model. Furthermore, a level of supersaturation of oxalate ion might be needed for the precipitation of a solid phase which is not considered in this model. This parameter might also

contribute to the underestimation of the model for RE_2Ox_3 precipitation run at the experimental concentrations.

5. Discussion

5.2 Leaching efficiency

The use of ionic solutions tested here has proven to be inefficient for the leaching of REY from umbers. Although this method is widely used in China for the treatment of REY adsorbed in clay with economic yields, a similar approach applied here resulted in only 0.3% REY recovery in optimal kinetic conditions. These results highlight a major difference between IAC and umber deposits considering REY location and binding within the deposit. Although REY were initially adsorbed on the surface of Fe and Mn oxides during umber deposition in the Tethyan Ocean, the REY can no longer be considered as easily exchangeable cations and stronger acid conditions are needed for their extraction. This can be partly in response to modifications in the structure and mineralogy of umbers induced by diagenesis of the deposits. Umbers comprise only minor goethite, quartz and zeolite, with amorphous Fe-Mn oxides still dominant suggesting that REY remain bound to the oxides, although they might be incorporated within the oxide matrix following diagenesis and cannot be substituted easily by ions of equivalent size at neutral pH.

5.1 REE leachability

In all acid leaching experiments, the mobilization of REY has been more efficient compared to the recovery of other minor elements scavenged by Fe and Mn oxides. The REY, in all oxidation states, have large ionic radii (0.86 - 1.04 Å), up to 60% larger, when compared to other cations potentially adsorbed like V (0.79 Å), Zn (0.74 Å), Cu (0.73 Å), Ni (0.69 Å) and Co (0.65 Å) in divalent state (Shannon, 1976). This difference in ionic size might account for their ease of extraction compared to these other elements, as they do not fit within the oxide structure as readily as other transition metals.

The upper limit for REY recovery, ~80-92% of the total REY content in the original sediment, emphasizes the distinction between REY loosely bound to amorphous oxides and those incorporated within the mineral structure of minor minerals formed during diagenesis such as goethite which are more resistant to the acid leach. The grain size of the material to be leached also constitutes an important parameter to take into account to improve recovery. This parameter can easily be adjusted in a processing plant and the crushing size will have a positive impact on the potential release of REY as the reaction area increases.

5.2 Optimal leaching conditions

Through the experiments carried out in laboratory conditions, all parameters tested indicates a kinetic control over the release of REY in the solution, approaching a maximum of 80 - 92% REY

extracted depending on the acid used. Threshold values when approaching asymptotes can be considered as the lowest conditions of the parameter tested to apply to optimize REY extraction for each parameter in the most cost-effective way. By implementing beyond threshold leaching settings of the n experiment within the n+1 test, optimal leaching conditions can be determined for an optimized REY extraction recipe considering acid concentration, pulp density, time of reaction and temperature. From the results reported here (Figure 1), it can be estimated that optimal extraction of REY from umbers can be achieved with either inorganic acid concentrated at 1 N, 70°C, SL ratio > 10 in 1 h on a shaking table that would give a yield equivalent or superior to 90% of the initial REY content (Table 6).

	Molarity				**LS ratio**				**Time**				**Temperature**	
	Treshold	Yield	max	Yield	Treshold	Yield	max	Yield	Treshold	Yield	max	Yield	max	Yield
	M	%	M	%	-	%	-	%	minutes	%	hours	%	°C	%
HNO_3	0.75	73	1.75	80	10	73	100	76	X	X	X	X	70	84
H_2SO_4	0.4	83	1.75	81	20	81	100	92	45	62	9	68	70	81
HCl	0.75	81	1.75	85	10	82	100	87	120	73	13	77	70	93

Table 6: Rare earth and yttrium yields from acid leaching experiments at the threshold (before asymptotic inflection) and maximum test parameter values.

This leaching process, when compared with industrial processes for the treatment of REY ore from alkaline rocks, pegmatites or carbonatites is relatively advantageous. It requires only low acid concentrations and near ambient temperatures, in contrast to cracking methods that employ concentrated acids and elevated temperatures (> 200 °C), and yields good performance considering no physical pre-concentration treatment is needed apart from crushing and pulverizing of the ore. Compared to IAC heap leaching (Vahidi *et al.*, 2016), the process applied for umbers treatment is relatively similar with an overall comparable efficiency although acid conditions are required. However, the umber leaching process requires only a few hours, in strong contrast to the 150 - 400 days required for IACs.

5.3 From Laboratory to industrial scale

The projection of these results obtained in laboratory experiments to the industrial scale should consider the following adjustments for processing costs reduction and optimization of the plant economic viability.

Optimal conditions for the leaching of umbers have shown that large volumes of acid are needed as 10:1 LS ratios are used. Implementing a distillation step following the leaching would allow recovering hydrochloric acid after condensing to recycle in the next batch (Figure 9). Here, the additional cost of heating up for distillation is counterbalanced by the significant reduction of volume of reactant needed on a long-term period. Furthermore, leaching efficiency is improved at higher temperatures and could therefore benefit from the higher temperature of distilled HCl.

Numerical modelling has demonstrated the importance of the initial leach REE concentration for the precipitation of oxalates. The higher the initial REE concentration the higher the precipitation efficiency. Therefore, the distillation and associated evaporation would induce an overconcentration of elements contained in the leach liquor and significantly increase oxalate precipitation efficiency that in turn would lead to a reduction in oxalate consumption.

Similar to HCl recycling, consumption of ammonium oxalate can be greatly reduced if the oxalate cake is digested by sodium hydroxide (Eq. 9). This reaction allows the conversion of REY oxalate into hydroxides and formation of sodium oxalate salts (Habashi, 2013) such that:

Eq. 9: $RE_2Ox_3 + 6NaOH^- \rightarrow 2RE(OH)_3 + Na_xOx_y$

The hydroxides are then calcined to form a mix REY oxide product and the sodium oxalate reintroduced as a reactant in the precipitation step (Figure 9).

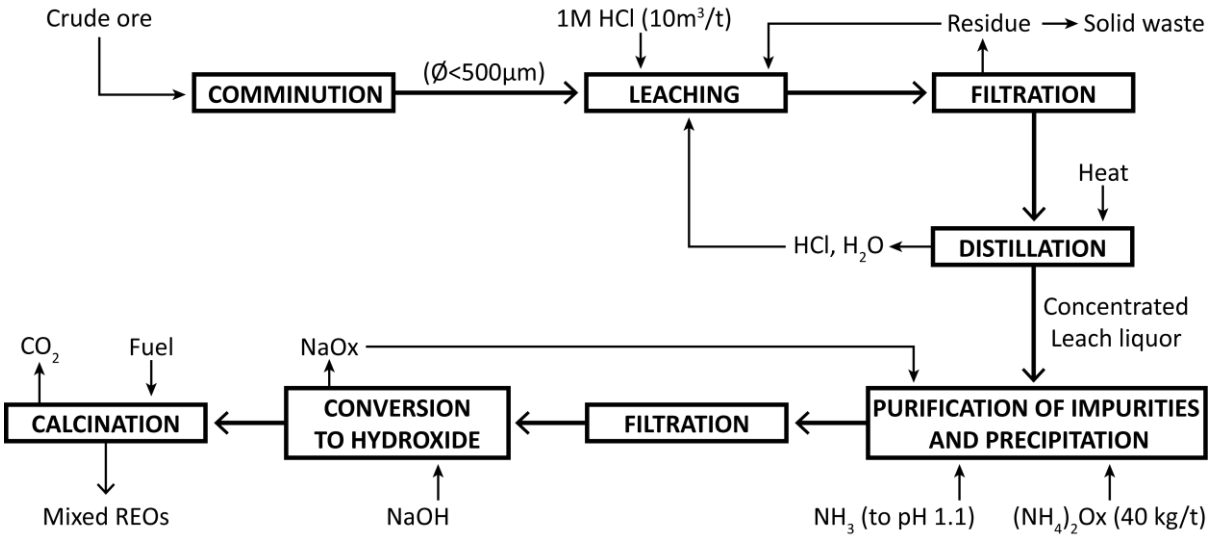

Figure 9: Optimized workflow of metalliferous sediment processing for the extraction of REY by simple acid leaching and oxalate precipitation.

5.3 Umber deposits as a potential REY resources in Cyprus and beyond

Umbers from Cyprus have been quarried extensively for pigments since ancient time and more recently for cement with a production decreasing from 30,000 tons per year in the late 70's to an average 6,000 tons per year in the last decade (Morse and Stevens, 1979, Cyprus Geological Survey, 2006). This reduction in umber exploitation is related to both the decrease in the use of umber as a natural pigment in paint or cement and to the great reduction of available, mineable umber accumulations. Most umber deposits in Cyprus comprise outcrops limited in size to tens of meters length for 1 or 2 meters thickness following the original paleo topography of the oceanic floor. Such outcrops are too dismembered to present any economic potential due to limited availability of the resource. However, incorporating REY production to the existing processing of umbers could bring an important value to such exploitation and reduce economic vulnerability by diversifying end-

products. This seems to be the strategy employed in a number of alternative deposits whereby REY extraction could be cost-effective from tailings as a by-product after main ore treatment such as processed bauxite (Tsakanika et al., 2004, Qu and Lian, 2013, Ujaczki *et al.*, 2015, Deady et al., 2016) or in coal residue (Rozelle *et al.*, 2016b). However, in the case of umbers, the extraction of REY by acid leaching has to happen as a first step and the residue can be neutralised, dried and sold as a pigment. Indeed, the leaching process using weak acid does not affect the overall mineralogy of umbers as REY are mainly associated with the amorphous oxide phase (Supplementary Figure 10) and the amount of leached Fe and Mn oxides, essential for the pigment quality, remains minor (< 3%).

Although umbers deposits in Cyprus are now too scarce to be economically viable, similar metalliferous sediment deposits can be found in most ophiolitic sequences preserved on land with significant tonnage to be considered of interest. Potential deposits include the multiple occurrences of umberiferous deposits in Japan, such as the Mineoka Hills (Kenzai Industrial Company), the Kunimiyama deposits in the Chichibu Belt, and the Mugi and Tyujin umbers in the Shimanto belt (Kato *et al.*, 2005a, Kato *et al.*, 2005b). These umber deposits are on average 4 m thick but commonly reach up to 12 m. With respect to Tethyan ophiolites, metalliferous ferromanganese sediments are found in association with many of the Eurasian Tethyan ophiolite complexes, but generally occur as small discrete bodies comparable to umbers in Troodos. Similar deposits are described from the Othris and Pindos Ophiolites (Greece) (Robertson and Varnavas, 1993b), the Kizildag (Hatay) Ophiolite (southern Turkey) (Robertson, 2002), or in the Semail Ophilite. The application of the hydrometallurgical process developed here for the Troodos umbers could be applied to these deposits given their similar nature, and therefore provide local sources for the production of rare earth metals.

6. Conclusions

Using Umbers, ferromanganese metalliferous sediments from the Troodos Ophiolite, as feedstock, the effectiveness of REY release in a leachate followed by selective precipitation was evaluated under different processing conditions.

In contrast to the liberation of REY from many of the current ore feedstock's, the extraction of rare earth elements from umbers by simple leaching using common industrial acids is effective without accumulation of radioactive by-products, and processes can be refined to maximise leaching efficiencies by adjusting acid concentration, temperature, pulp density and time of reaction. Although ionic solutions such as sodium chloride or ammonium sulphate are widely used in China for the treatment of ion adsorption clays, such approaches were not effective for leaching REY, demonstrating that REY could not be considered as easily exchangeable cations in umbers, and that stronger acid conditions are necessary for their extraction. Acid-promoted REY release displays

hyperbolic trends of recovery for all kinetic parameters tested. REY constitute the most susceptible elements to the leaching conditions tested with recovery reaching 80-92% of the sample content in optimized conditions. Main impurities included in the leach solutions are Mn, Ca, Fe and Na by weight but Ca and Na show proportionally the highest recovery rate. The leaching stage therefore produces an enrichment factor ranging from 50 to 75 for REY from sample to leach solution. A two-stage leaching process using HCl is an efficient method to separate most of the contaminants (Ca, Na) into the first leach. However, around 20% of the total REY content of the sample is also leached out which represents an important loss given the low purity of the initial ore. Therefore, the valuable improvements in purity of the second leach must be balanced against significant reductions in yields of the targeted elements in the second leach.

The use of oxalate is an efficient way of precipitating REY from acid leach liquor with more than 96% of the total REY content precipitated between pH 1 and 2. The strong dependence on pH for precipitation of diverse chemical species allows for the selective precipitation of REY from other impurities. The purity is optimal at pH 1.1 as abundant Ca-oxalate precipitates at higher pH. The fractionation observed between the different rare earth elements in the experiment was successfully explained via numeric modelling using PHREEQC: (i) the increasing recoveries from L- to M-REE and decreasing trends towards the HREE at pH < 1.5 follow the solid RE-oxalate solubility constant distribution -log β ($RE_2Ox_3.nH_2O$), (ii) the decreasing recovery trends at pH > 2 results from competition with Ca oxalate formation, (iii) the decrease in the recovery is not as steep in the experiment as it is in the model due to co-precipitation of REY with the Ca-oxalate phase or other phases not taken into account in the model. In addition, the model predicts an optimal pH window for the precipitation of REY between 0.9 and 1.1 because of oxalic acid dissociation, availability of Ox^{2-} and lack of competing ions.

With REO concentrations reaching 0.06 wt.%, umbers are low grade, and far below concentrations encountered in main magmatic primary deposits. However, REO contents of umber deposits are within the range of concentrations encountered in IAC deposits (Yang et al., 2013) and many active mines from which REE are processed as by-products (Graedel et al., 2014). In contrast to the numerous processing steps of these active REY mines, a REY precipitate of high purity (> 70% REY) can be produced from umber deposits rapidly in only two-steps and with extremely low radioactive content.

These experimental results and modelling confirm previous views on the beneficiation potential of deep-sea sediments potential as a REY resource (Kato et al., 2011, Fujimoto et al., 2016, Menendez et al., 2017) as well as red-mud- or coal-processing residue (Qu and Lian, 2013, Deady et al., 2016, Rozelle et al., 2016a) considered as raw polymetallic materials. These results expand the list of potential REY resource available by integrating oceanic hydrothermal metalliferous deposits preserved on-land.

Acknowledgements

This research was funded by the Southampton Marine & Maritime Institute (SMMI), the Graduate School of the National Oceanography Centre (GSNOC), the Faculty of Engineering and the Environment of Southampton University and the Natural History Museum of London with PhD Scholarship to Pierre Josso from the SMMI and GSNOC. The authors would like to thank J. Schijf, J. Declercq and P. Warwick for their encouraging comments and help throughout the chemical modelling, M. Cooper for his assistance in the laboratory work, R. Williams for the XRD analysis and R. Pearce for his assistance on the SEM.

References

Abreu, R. D. & Morais, C. A. 2010. Purification of rare earth elements from monazite sulphuric acid leach liquor and the production of high-purity ceric oxide. *Minerals Engineering,* 23**,** 536-540.

Abreu, R. D. & Morais, C. A. 2014. Study on separation of heavy rare earth elements by solvent extraction with organophosphorus acids and amine reagents. *Minerals Engineering,* 61**,** 82-87.

Bau, M. & Koschinsky, A. 2009. Oxidative scavenging oc cerium on hydrous Fe oxide: Evidence from the distributionof rare earth elements and yttrium between Fe oxides and Mn oxides in hydrogenetic ferromanganese crusts. *Geochemical Journal,* 43**,** 37-47.

Bhat, T. R. & Rao, T. V. 1964. Solubilities of Rare Earth Oxalates in EDTA Solutions and the Determination of their Solubility Products. *Zeitschrift fiir nnorganisclie nnd allgemeine Chemie,* 332**,** 204-208.

Borra, C. R., Pontikes, Y., Binnemans, K. & Van Gerven, T. 2015. Leaching of rare earths from bauxite residue (red mud). *Minerals Engineering,* 76**,** 20-27.

Boyle, J. F. 1984. *The origin and geochemistry of the metalliferous sediments of the Troodos massif, Cyprus.* Doctor of Philosophy, University of Edinburgh.

Boyle, J. F. & Robertson, A. H. F. 1984. Evolving metallogenesis at the Troodos spreading axis. *Geological Society, London, Special Publications,* 13**,** 169-181.

Boyle, J. F. 1990. The composition and origin of metalliferous sediments from the Troodos ophiolite, Cyprus. *In:* MALPAS, J. (ed.) *Ophiolites: oceanic crustal analogues, Proceedings of the Symposium "Troodos" 1987: Nicosia, Cyprus.* Geological Survey, p. 705-718.

Chakhmouradian, A. R. & Wall, F. 2012. Rare Earth Elements: Minerals, Mines, Magnets (and More). *Elements,* 8**,** 333-340.

Chi, R., Xu, J., He, P. & Zhu, Y. 1995. Recovering RE From Leach Liquor of Rare Earth Ore by Extraction. *Transactions of NFsoc,* 5**,** 5.

Chi, R. & Xu, Z. 1998. A Solution Chemistry Approach to the Study of Rare Earth Element Precipitation by Oxalic Acid. *Metallurgical and Materials Transactions,* 30B.

Christie, T., Brathwaite, B. & Tulloch, A. 1998. Rare Earths and Related Elements. *Mineral Comodity Report 17.*

Chung, D. Y., Kim, E. H., Lee, E. H. & Yoo, J. H. 1998. Solubility of Rare Earth Oxalate in Oxalic and Nitric Acid Media. *Journal of Industrial and Engineering Chemistry,* 4**,** 277-284.

Crouthamel, C. E. & Martin, D. S. 1951. Solubility of the Rare Earth Oxalates and Complex Ion Formation in Oxalate Solution. II. Neodoymium and Cerium (III). *Journal of the American Chemical Society,* 72**,** 1382-1386.

Cyprus Geological Survey 2006. Report on raw materials mineral production in Cyprus. Ministry of Agriculture Natural Resources and Environment.

Deady, E. A., Mouchos, E., Goodenough, K. M., Williamson, B. J. & Wall, F. 2016. A review of the potential for rare-earth element resources from European red muds: examples from Seydişehir, Turkey and Parnassus-Giona, Greece. *Mineralogical Magazine,* 80**,** 43-61.

Delany, J. M. & Lundeen, S. R. 1990. The LLNL thermochemical database. *Lawrence Livermore Natl. Lab. Livermore, CA***,** 150p.

European Commission 2014. Report on critical materials for the EU. *Report of the Ad hoc Working Group on defining critical raw materials.* Brussels.

Feibush, A. M., Rowley, K. & Gordon, L. I. 1958. Solubility of Yttrium Oxalate. *Analytical Chemistry,* 30**,** 1610-1612.

Fujimoto, J., Tanaka, K., Watanabe, N. & Takahashi, Y. 2016. Simultaneous recovery and separation of rare earth elements in ferromanganese nodules by using Shewanella putrefaciens. *Hydrometallurgy*.

Golev, A., Scott, M., Erskine, P. D., Ali, S. H. & Ballantyne, G. R. 2014. Rare earths supply chains: Current status, constraints and opportunities. *Resources Policy,* 41**,** 52-59.

Goodenough, K. M., Schilling, J., Jonsson, E., Kalvig, P., Charles, N., Tuduri, J., Deady, E. A., Sadeghi, M., Schiellerup, H., Müller, A., Bertrand, G., Arvanitidis, N., Eliopoulos, D. G., Shaw, R. A., Thrane, K. & Keulen, N. 2016. Europe's rare earth element resource potential:

An overview of REE metallogenetic provinces and their geodynamic setting. *Ore Geology Reviews,* 72, Part 1**,** 838-856.
Graedel, T. E., Gunn, G. & Tercero Espinoza, L. 2014. Metal resources, use and Criticality. *Critical Metals Handbook.* John Wiley & Sons.
Grenthe, I., Gardhammar, G. & Rundcrantz, E. 1969. Thermodynamic Properties of Rare Earth Complexes VI. Stability Constants for the Oxalate Compelxes of Ce (III), Eu (III), Tb (III), and Lu (III). *Acta Chemica Scandinavica,* 23**,** 93-108.
Guyonnet, D., Planchon, M., Rollat, A., Escalon, V., Tuduri, J., Charles, N., Vaxelaire, S., Dubois, D. & Fargier, H. 2015. Material flow analysis applied to rare earth elements in Europe. *Journal of Cleaner Production,* 107**,** 215-228.
Habashi, F. 2013. Extractive Metallurgy of Rare Earths. *Canadian Metallurgical Quarterly,* 52**,** 224-233.
Hansson, E. 1970. Structural studies on the Rare Earth Carboxylates: The crystal and molecular structure of neodymium (III) oxalate 10.5-hydrate. *Acta Chemica Scandinavica,* 24**,** 2969-2982.
Hein, J. R., Mizell, K., Koschinsky, A. & Conrad, T. A. 2013. Deep-ocean mineral deposits as a source of critical metals for high- and green-technology applications: Comparison with land-based resources. *Ore Geology Reviews,* 51**,** 1-14.
Hoshino, M., Sanematsu, K. & Watanabe, Y. 2016. REE Mineralogy and Resources. *Handbook on the Physics and Chemistry of Rare Earths,* 49**,** 129-291.
Jaireth, S., Hoatson, D. M. & Miezitis, Y. 2014. Geological setting and resources of the major rare-earth-element deposits in Australia. *Ore Geology Reviews,* 62**,** 72-128.
Jochum, K. P., Nohl, U., Herwig, K., Lammel, E., Stoll, B. & Horfmann, A. 2005. *Geostandards and Geoanalytical Research*.
Jordens, A., Cheng, Y. P. & Waters, K. E. 2013. A review of the beneficiation of rare earth element bearing minerals. *Minerals Engineering,* 41**,** 97-114.
Josso, P. 2017. *Investigating the potential recovery of REY from metalliferous sediments in a seafloor analogue; The Troodos ophiolite, Cyprus.* PhD Thesis, University of Southampton.
Kanazawa, Y. & Kamitani, M. 2006. Rare earth minerals and resources in the world. *Journal of Alloys and Compounds,* 408–412**,** 1339-1343.
Kato, Y., Fujinaga, K., Nozaki, T., Osawa, H., Nakamura, K. & Ono, R. 2005a. Rare earth, Major and Trace Elements in the Kunimiyama Ferromanganese Deposit in the Northern Chichibu Belt, Central Shikoku, Japan. *Resource Geology,* 55**,** 291-299.
Kato, Y., Fujinaga, K. & Suzuki, K. 2005b. Major and trace element geochemistry and Os isotopic composition of metalliferous umbers from the Late Cretaceous Japanese accretionary complex. *Geochemistry Geophysics Geosystems,* 6**,** 20p.
Kato, Y., Fujinaga, K., Nakamura, K., Takaya, Y., Kitamura, K., Ohta, J., Toda, R., Nakashima, T. & Iwamori, H. 2011. Deep-sea mud in the Pacific Ocean as a potential resource for rare-earth elements. *Nature Geoscience,* 4**,** 535-539.
Kolo, M. T., Aziz, S. a. B. A., Khandaker, M. U., Asaduzzaman, K. & Amin, Y. M. 2015. Evaluation of radiological risks due to natural radioactivity around Lynas Advanced Material Plant environment, Kuantan, Pahang, Malaysia. *Environmental Science and Pollution Research,* 22**,** 13127-13136.
Koschinsky, A. & Halbach, P. 1995. Sequential leaching of marine ferromanganese precipitates: Genetic implications. *Geochimica and Cosmochimica Acta,* 59**,** 5113-5132.
Koschinsky, A. & Hein, J. R. 2003. Uptake of elements from seawater by ferromanganese crusts: solid-phase associations and seawater speciation. *Marine Geology,* 198**,** 331-351.
Kumar, V., Jha, M. K., Kumari, A., Panda, R., Kumar, J. R. & Lee, J. Y. 2014. Recovery of rare earth metals (REMs) from primary and secondary resources: a review. *In:* NEELAMEGGHAM, N. R., ALAM, S., OOSTERHOF, H., JHA, A. & WANG, S. (eds.) *rare Metal technology.* The minerals, Metals & Materials Society.
Liu, Y. & Naidu, R. 2014. Hidden values in bauxite residue (red mud): Recovery of metals. *Waste Management,* 34**,** 2662-2673.
Martell, A. E. & Smith, R. M. 1977. Critical Stability Constants, Vol. 3, other Organic Ligands Plenum.
Martell, A. E. & Smith, R. M. 1982. Critical Stability Constants, Vol. 5, First Supplement Plenum. 5.

916 Menendez, A., James, R. H., Roberts, S., Peel, K. & Connelly, D. 2017. Controls on the distribution
917 of rare earth elements in deep-sea sediments in the North Atlantic Ocean. *Ore Geology*
918 *Reviews,* 87**,** 100-113.
919 Morse, D. E. & Stevens, C. 1979. The Mineral Industry of Cyprus. *Minerals Yearbook***,** 283-288.
920 Ochsenkühn-Petropulu, M., Lyberopulu, T., Ochsenkühn, K. M. & Parissakis, G. 1996. Recovery of
921 lanthanides and yttrium from red mud by selective leaching. *Analytica Chimica Acta,* 319**,**
922 249-254.
923 Parkhurst, D. L. & Appelo, C. a. J. 2013. Description of input and examples for PHREEQC version 3:
924 a computer program for speciation, batch-reaction, one-dimensional transport, and
925 inverse geochemical calculations. U. S. Geological Survey, Techniques and Methods, pp.
926 497.
927 Qu, Y. & Lian, B. 2013. Bioleaching of rare earth and radioactive elements from red mud using
928 Penicillium tricolor RM-10. *Bioresource Technology,* 136**,** 16-23.
929 Rao, C. N. R., Natarajan, S. & Vaidhyanathan, R. 2004. Metal Carboxylates with open architectures.
930 *Angewandte Chemie,* 43**,** 1466-1496.
931 Richards, H. G. & Boyle, J. F. 1986. Origin, alteration and mineralization of inter-lava metalliferous
932 sediments of the Troodos Ophiolite, Cyprus. *In:* GALLAGHER, M. J., IXER, R. A., NEARY, C.
933 R. & PRICHARD, H. M. (eds.) *Proceedings of the conference 'Metallogeny of basic and*
934 *ultrabasic rocks'. Edimburgh, Scotland, from 9 to 12 April, 1985.*
935 Robertson, A. H. F. & Hudson, J. D. 1972. Cyprus umbers: chemical precipitates on a thetyan
936 ocean ridge. *Earth and Planetary Science Letters,* 18**,** 93-101.
937 Robertson, A. H. F. & Hudson, A. 1974. Pelagic sediments in the Cretaceous and Tertiary history of
938 the Troodos Massif, Cyprus. *Special publication of the International Association of*
939 *Sedimentology,* 1**,** 403-436.
940 Robertson, A. H. F. & Varnavas, S. P. 1993a. The origin of hydrothermal metalliferous sediments
941 associated with the early Mesozoic Othris and Pindos ophiolites, mainland Greece.
942 *Sedimentary Geology,* 83**,** 87-113.
943 Robertson, A. H. F. & Varnavas, S. P. 1993b. The origin of hydrothermal metalliferous sediments
944 associated with the Early Mesozoic Othris and Pindos ophiolites, mainland Greece.
945 *Sedimentary Geology,* 83**,** 87-113.
946 Robertson, A. H. F. 2002. Overview of the genesis and emplacement of Mesozoic ophiolites in the
947 Eastern Mediterranean Tethyan region. *Lithos,* 65**,** 1-67.
948 Rollat, A., Guyonnet, D., Planchon, M. & Tuduri, J. 2016. Prospective analysis of the flows of
949 certain rare earths in Europe at the 2020 horizon. *Waste Management,* 49**,** 427-436.
950 Rozelle, P. L., Khadilkar, A. B., Pulati, N., Soundarrajan, N., Klima, M. S., Mosser, M. M., Miller, C. E.
951 & Pisupati, S. V. 2016a. A Study on removal of Rare Earth Elements from U.S. Coal
952 Byproducts by Ion Exchange. *Metallurgical and Materials Transactions E 3***,** 6-17.
953 Rozelle, P. L., Khadilkar, A. B., Pulati, N., Soundarrajan, N., Klima, M. S., Mosser, M. M., Miller, C. E.
954 & Pisupati, S. V. 2016b. A Study on removal of Rare Earth Elements from U.S. Coal
955 Byproducts by Ion Exchange. *Metallurgical and Materials Transactions***,** 12p.
956 Salman, H. M., El Hussaini, O. M., Abd-El Fatah, N. A. & Mahmoud, M. S. 2014. Extraction of
957 yttrium from ferruginous sandstone, Southwestern Sinai, Egypt. *The Journal of Applied*
958 *Sciences Research,* 1**,** 173-182.
959 Schijf, J. & Byrne, R. H. 2001. Stability constant for mono- and dioxalato-complexes of Y and REE,
960 potentially important species in groundwaters and surface waters. *Geochimica and*
961 *Cosmochimica Acta,* 65**,** 1037-1046.
962 Shannon, R. D. 1976. Revised effective ionic radii and systematic studies of interatomic distances
963 in halides and chalcogenides. *Acta Crystaloographica,* 32**,** 751-767.
964 Smith, R. M. & Martell, A. E. 2004. NIST Critically Selected Stability Constants of Metal Complexes
965 Database. Version 8.0 for Windows. National Institute of Standards and Technology, Texas
966 A&M University.
967 Tsakanika, L. V., Ochsenkühn-Petropoulou, M. T. & Mendrinos, L. N. 2004. Investigation of the
968 separation of scandium and rare earth elements from red mud by use of reversed-phase
969 HPLC. *Analytical and Bioanalytical Chemistry,* 379**,** 796-802.

970 Ujaczki, E., Zimmermann, Y. S., Feigl, V. & Lenz, M. 2015. Recovery of rare earth elements from
971 Hungarian red mud with combined acid leaching and liquid-liquid extraction. *Bauxite*
972 *residue valorisation and best practices.* Leuven 5-7 October 2015.
973 Vahidi, E., Navarro, J. & Zhao, F. 2016. An initial life cycle assessment of rare earth oxides
974 production from ion-adsorption clays. *Resources, Conservation and Recycling,* 113**,** 1-11.
975 Vander Hoogerstraete, T., Blanpain, B., Van Gerven, T. & Binnemans, K. 2014. From NdFeB
976 magnets towards the rare-earth oxides: a recycling process consuming only oxalic acid.
977 *RSC Advances,* 4**,** 64099-64111.
978 Weng, Z., Jowitt, S. M., Mudd, G. M. & Haque, N. 2015. A Detailed Assessment of Global Rare
979 Earth Element Resources: Opportunities and Challenges. *Economic Geology,* 110**,** 1925-
980 1952.
981 Xie, F., Zhang, T. A., Dreisinger, D. & Doyle, F. 2014. A critical review on solvent extraction of rare
982 earths from aqueous solutions. *Minerals Engineering,* 56**,** 10-28.
983 Xiong, Y. 2011. Organic species of lanthanum in natural environments: Implications to mobility of
984 rare earth elements in low temperature environments. *Applied Geochemistry,* 26**,** 1130-
985 1137.
986 Yang, X. J., Lin, A., Li, X. L., Wu, Y., Zhou, W. & Chen, Z. 2013. China's ion-adsorption rare earth
987 resources, mining consequences and preservation. *Environmental Development,* 8**,** 131-
988 136.
989 Zinin, D. S. & Bushuev, N. N. 2014. Production and physicochemical study of oxalate and oxide REE
990 concentrates. *Russian Journal of Applied Chemistry,* 87**,** 1611-1618.

991

992 **Supplementary data**

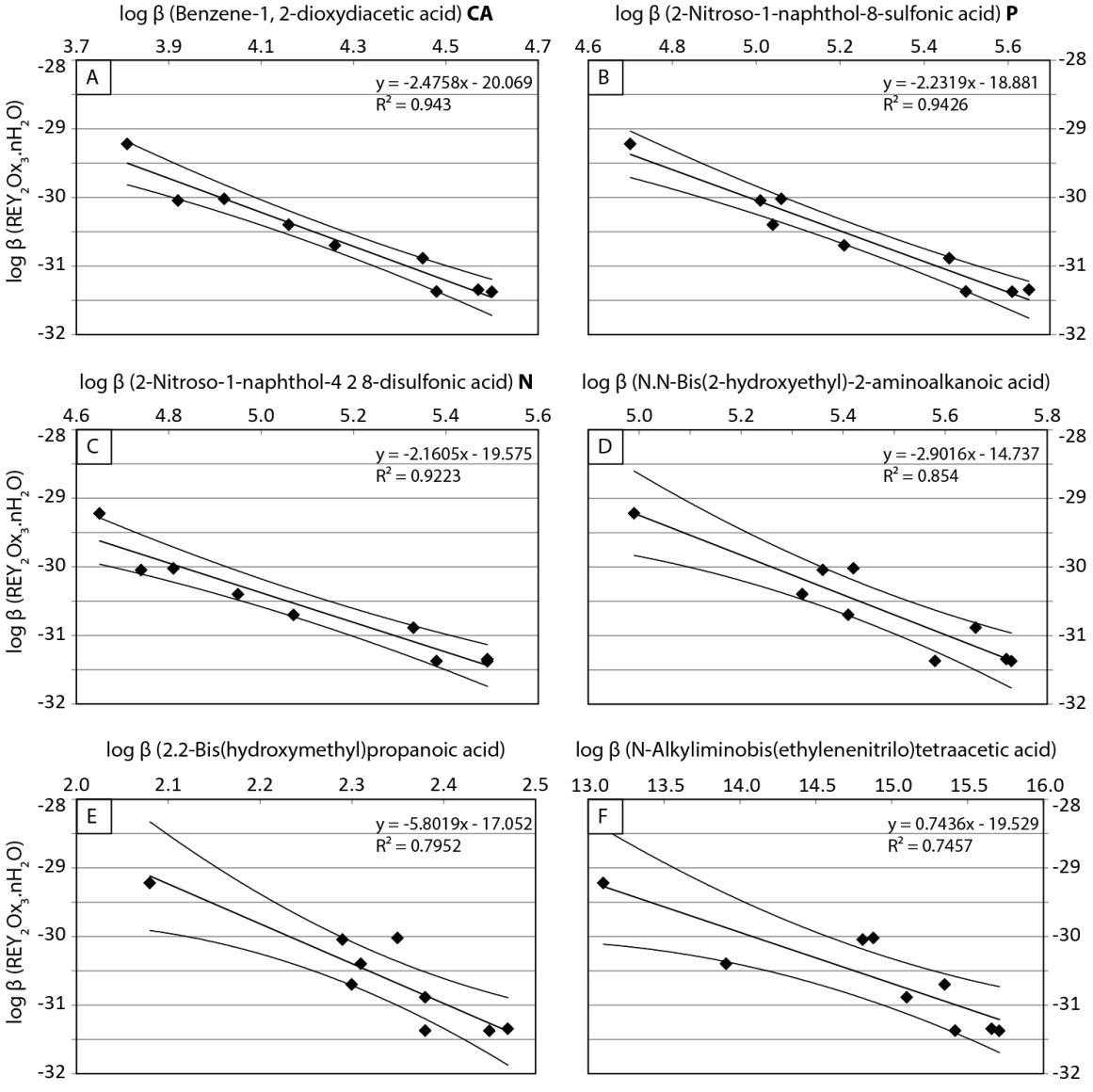

993

994 Supplementary Figure 1: Linear free-energy relationships for $RE_2Ox_3.nH_2O$ oxalate complexes with various
995 organic acids. Displayed on graphs are equation of linear regression with R^2 values and 95% CI on the linear
996 regression.

997

	grain size (µm) per fraction (x %) of the sample								
Sample PJ-CY-91	5%	10%	16%	20%	50%	80%	84%	90%	95%
A1-1	2.3	3.5	5.9	8.6	101.3	279.4	314.7	387.9	486.9
A1-2	2.1	3.3	5.2	7.6	87.9	258.0	292.1	368.7	473.8
A1-3	2.2	3.5	5.9	8.7	99.1	277.4	317.8	432.1	724.5
Avg. 1st aliquot	2.2	3.5	5.7	8.3	95.8	271.5	308.1	391.2	525.6
A2-1	2.5	3.6	5.3	6.8	58.7	224.8	255.3	319.4	539.5
A2-2	2.4	3.6	5.1	6.6	53.0	217.1	250.5	330.2	596.1
A2-3	2.5	3.7	5.5	7.2	59.0	229.3	265.2	380.9	592.5
Avg. 2nd aliquot	2.5	3.6	5.3	6.9	56.9	223.6	256.8	336.7	577.7
Average ± σ	2.3 ± 0.1	3.4 ± 0.1	5.5 ± 0.3	7.6 ± 0.8	76.5 ± 20.1	247.7 ± 25.2	282.6 ± 27.2	369.9 ± 37.5	568.9 ± 83.8

998

999 Supplementary Table 1: Grain size measurement (in µm) for two aliquots of sample PJ-CY-91. Values
1000 represent the maximum size of particles for a fixed fraction of the sample.

1001

All values expressed in mg/kg

	average (n = 3)	BHVO2[a]	average (n = 3)	BIR1[a]	average (n = 3)	JB3[a]
Na	15588 ± 381	15262 - 16100	12513 ± 522	13550	19498 ± 958	20400
Mg	42878 ± 2125	38853 - 43600	57440 ± 1480	54752 - 60300	30818 ± 821	20321 - 34431
Al	69812 ± 3701	70062 - 71600	81122 ± 2005	79244 - 85434	90122 ± 2690	85381 - 94215
K	4696 ± 480	4280 - 5080	266.6 ± 31	198 - 250	6735 ± 489	6000
Ca	80522 ± 2796	78087 - 82440	96502 ± 3421	94000 - 97281	68505 ± 4087	70000
Ti	16405 ± 227	15113 - 27300	5736 ± 74	4875 - 6923	8460 ± 98	8842
Mn	1338 ± 42	1020 - 1432	1383 ± 41	1278 - 1414	1473 ± 49	1263 - 1355
Fe	88263 ± 286	71293 - 83865	84672 ± 4468	68668 - 79900	87855 ± 3379	82500 - 83689
Sc	31.0 ± 0.8	32	41.7 ± 0.7	41 - 45	33.1 ± 0.4	32 - 35.9
Co	43.1 ± 0.6	34 - 56.2	50.0 ± 1.2	41.3 - 64.2	34.5 ± 1.3	24 - 43.3
Ni	118.5 ± 3.3	97.9 - 186	168.2 ± 6.6	116.7 - 249.5	37.6 ± 2.1	32 - 49.1
Cu	130.6 ± 3.6	102 - 168	119.0 ± 4.2	97.3 - 152	193.4 ± 9.4	142 - 196
Sr	427.3 ± 9.7	317 - 438.3	105.7 ± 5.1	90 - 130	442.1 ± 6.2	392 - 452
Y	23.6 ± 1.2	18.8 - 30.4	14.1 ± 0.7	11.28 - 18	23.6 ± 1.1	21.7 - 28.6
Zr	161.2 ± 12.8	124.5 - 195.3	13.4 ± 0.9	4.87 - 32.87	87.5 ± 5.8	86.2 - 110.43
Ba	131.0 ± 5.2	99 - 150	6.4 ± 0.2	0.635 - 17.2	239.8 ± 7.6	217 - 271
La	15.00 ± 0.84	13 - 16.9	0.60 ± 0.03	0.36 - 3.6	8.37 ± 0.40	7.65 - 10.18
Ce	37.80 ± 1.94	32.41 - 45.3	1.90 ± 0.09	1 - 4.44	21.44 ± 0.97	19.5 - 56
Pr	5.27 ± 0.35	4.72 - 5.93	0.37 ± 0.03	0.10 - 0.46	3.21 ± 0.20	3 - 5
Nd	25.11 ± 1.05	22.36 - 28.1	2.46 ± 0.10	1.6 - 3.3	16.17 ± 0.59	14.5 - 17.03
Sm	6.34 ± 0.25	5.14 - 6.9	1.15 ± 0.05	0.8 - 1.24	4.42 ± 0.17	2.95 - 4.83
Eu	2.14 ± 0.11	1.71 - 2.7	0.54 ± 0.03	0.3 - 0.6	1.37 ± 0.07	1.24 - 1.6
Gd	6.41 ± 0.34	4.68 - 7.34	1.94 ± 0.10	0.36 - 3.2	4.81 ± 0.24	3.9 - 5.2
Tb	0.97 ± 0.06	0.72 - 1.08	0.38 ± 0.02	0.22 - 2.28	0.76 ± 0.05	0.65 - 0.94
Dy	5.61 ± 0.31	4.03 - 6.05	2.74 ± 0.14	2.5 - 4	4.85 ± 0.25	3.9 - 4.98
Ho	1.03 ± 0.06	0.7 - 1.12	0.61 ± 0.03	0.34 - 0.64	0.99 ± 0.05	0.82 - 1
Er	2.69 ± 0.16	1.7 - 2.82	1.84 ± 0.11	1 - 1.89	2.86 ± 0.16	2.39 - 2.88
Tm	0.35 ± 0.02	0.26 - 0.42	0.27 ± 0.02	0.14 - 0.3	0.41 ± 0.02	0.34 - 0.59
Yb	2.13 ± 0.13	1.59 - 2.38	1.80 ± 0.10	1.36 - 1.8	2.68 ± 0.14	2.2 - 2.83
Lu	0.30 ± 0.02	0.2 - 0.38	0.28 ± 0.02	0.18 - 0.31	0.40 ± 0.02	0.32 - 0.5
Th	1.30 ± 0.06	1.03 - 3.51	0.05 ± 0.00	0.03	1.34 ± 0.05	1 - 1.42
U	0.45 ± 0.02	0.32 - 0.51	0.02 ± 0.00	0.031	0.52 ± 0.03	0.47 - 0.54

1002 Standard[a], published values from Jochum et al., [2005]

1003 Supplementary Table 2: Average ± 95 % CI of measured trace element concentration of rock standards run
1004 as triplicates and their recommended published values for accuracy and reproducibility checking.

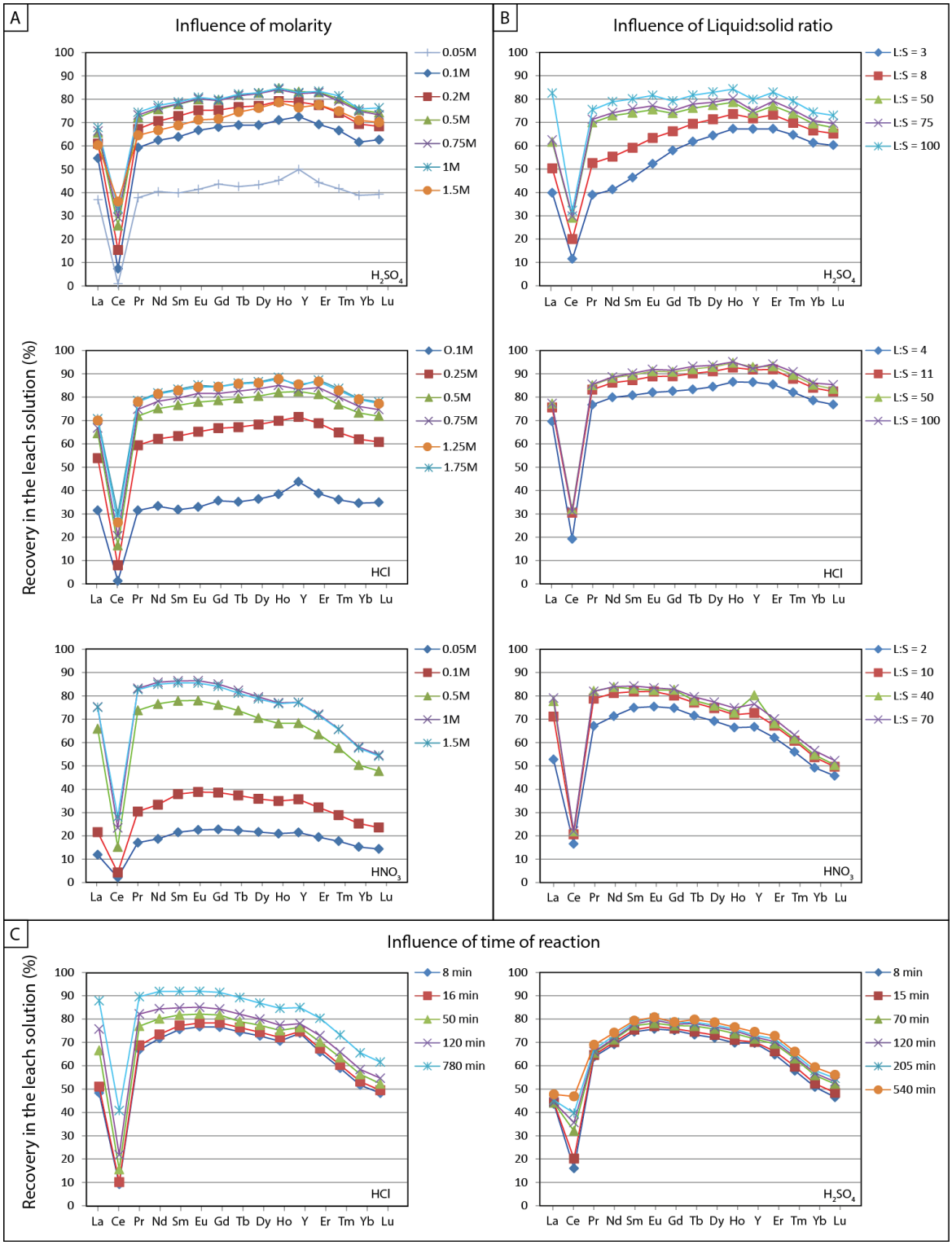

Supplementary Figure 2: Detailed recovery for REY in each leaching experiment.

	pH 1.1 no HF treatment					
	Bulk	**area_Xlarge**	**spot_Xlarge**	**area_Xsmall**	**spot_Xsmall**	**area_Xlarge_2**
	Wt.% ± σ	Wt.% ± σ	Wt.% ± σ	Wt.% ± σ	Wt.% ± σ	Wt.% ± σ
Si	1.2 ± 0.1	0.9 ± 0.1	-	0.5 ± 0.1	0.5 ± 0.1	-
Cl	1.5 ± 0.1	4.0 ± 0.2	1.7 ± 0.1	1.7 ± 0.1	5.4 ± 0.2	-
K	-	0.5 ± 0.1	-	-	-	-
Ca	6.9 ± 0.2	8.7 ± 0.2	8.9 ± 0.2	5.0 ± 0.1	6.2 ± 0.2	3.7 ± 0.1
Al	3.9 ± 0.3	0.8 ± 0.2	0.9 ± 0.2	0.7 ± 0.2	0.7 ± 0.2	0.7 ± 0.2
Cu	1.0 ± 0.2	-	-	-	-	1.1 ± 0.2
Y	16.6 ± 0.6	15.3 ± 0.6	10.0 ± 0.4	10.8 ± 0.4	11.2 ± 0.5	23.2 ± 0.6
La	16.4 ± 0.5	18.5 ± 0.5	19.5 ± 0.5	19.8 ± 0.4	18.1 ± 0.5	18.0 ± 0.5
Ce	4.0 ± 0.4	4.6 ± 0.4	4.4 ± 0.4	4.9 ± 0.4	4.8 ± 0.4	4.0 ± 0.4
Pr	6.2 ± 0.5	6.1 ± 0.5	6.1 ± 0.5	7.4 ± 0.5	7.2 ± 0.5	5.9 ± 0.5
Nd	25.9 ± 0.6	26.5 ± 0.6	30.2 ± 0.6	29.2 ± 0.5	29.7 ± 0.6	26.3 ± 0.6
Sm	5.5 ± 0.5	5.5 ± 0.5	6.2 ± 0.5	6.9 ± 0.5	5.6 ± 0.5	5.9 ± 0.5
Gd	5.6 ± 0.5	5.3 ± 0.5	6.3 ± 0.5	6.4 ± 0.5	6.5 ± 0.5	5.4 ± 0.5
Dy	3.7 ± 0.5	3.4 ± 0.5	4.2 ± 0.5	5.0 ± 0.4	4.2 ± 0.5	3.9 ± 0.5
Er	1.7 ± 0.5	-	1.7 ± 0.5	1.6 ± 0.5	± 0.0	1.8 ± 0.5
REY	85.6 ± 0.5	85.1 ± 0.5	88.5 ± 0.5	92.0 ± 0.5	87.3 ± 0.5	94.5 ± 0.5

Supplementary Table 3: Energy-dispersive X-ray spectroscopy analysis of the oxalate precipitates at pH 1.1. Note that EDS analysis were made on a free C and O basis. Area and crystals analysed are displayed in **Error! Reference source not found.**.

	pH 2.5 no HF			pH 2.5 with HF treatment	
	Bulk	**spot-Xlarge**	**spot-Xsmall**	**Bulk**	**spot_Xlarge**
	Wt.% ± σ	Wt.% ± σ	Wt.% ± σ	Wt.% ± σ	Wt.% ± σ
F	-	-	-	5.7 ± 1.4	3.0 ± 0.9
Na	1.1 ± 0.2	1.2 ± 0.2	1.4 ± 0.3	0.0 ± 0.0	0.9 ± 0.2
Cl	0.8 ± 0.1	1.1 ± 0.1	1.3 ± 0.1	2.0 ± 0.1	1.0 ± 0.1
Ca	80.6 ± 0.7	83.7 ± 0.7	84.9 ± 0.7	78.0 ± 1.4	81.9 ± 0.7
Mn	7.4 ± 0.3	7.4 ± 0.3	7.6 ± 0.3	3.0 ± 0.3	7.4 ± 0.3
Al	4.9 ± 0.3	0.8 ± 0.2	0.6 ± 0.1	4.3 ± 0.2	0.9 ± 0.1
Cu	0.6 ± 0.2	-	-	0.8 ± 0.1	-
Sr	0.9 ± 0.3	0.7 ± 0.3	0.0 ± 0.0	-	1.0 ± 0.3
Y	1.0 ± 0.4	1.8 ± 0.4	1.0 ± 0.4	1.2 ± 0.4	1.4 ± 0.4
La	1.5 ± 0.4	1.5 ± 0.4	1.7 ± 0.4	2.9 ± 0.4	2.8 ± 0.4
Nd	1.2 ± 0.4	1.7 ± 0.4	1.4 ± 0.4	2.2 ± 0.5	2.8 ± 0.4
REY	3.7 ± 0.4	5.0 ± 0.4	4.2 ± 0.4	6.3 ± 0.5	7.0 ± 0.4

Supplementary Table 4: Energy-dispersive X-ray spectroscopy analysis of the oxalate precipitates at different pH. Note that EDS analysis were made on a free C and O basis. Area and crystals analysed are displayed in **Error! Reference source not found.**.

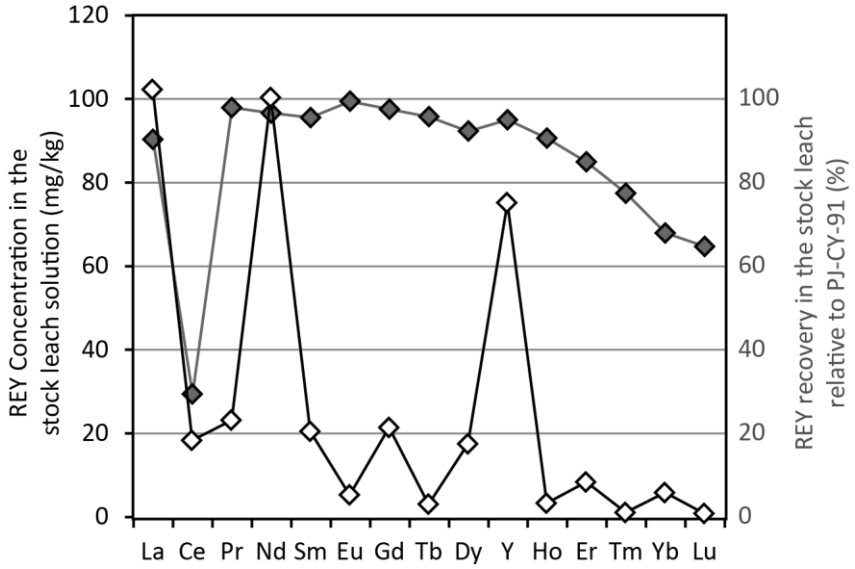

1020

1021 Supplementary Figure 3: REY concentration in the leaching solution (white diamond, scale on the left) and
1022 the relative elemental recovery from the sample (grey diamond, scale on the right).

1023

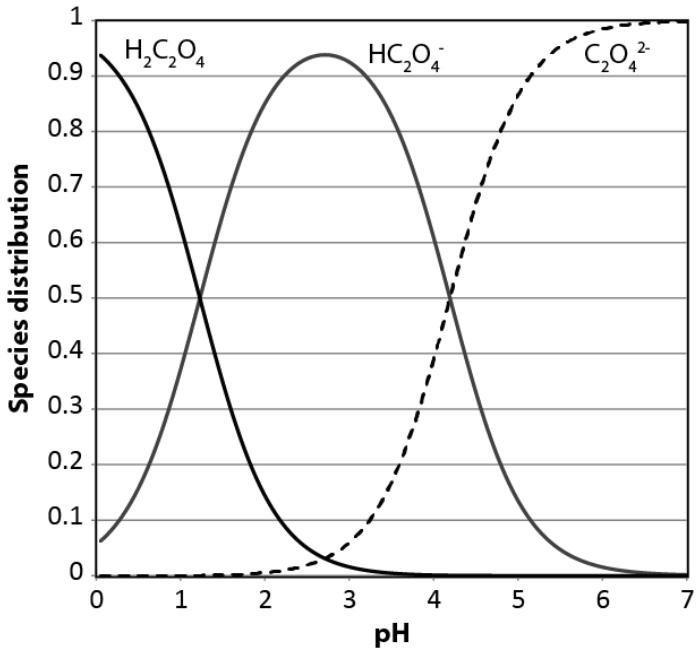

1024

1025 Supplementary Figure 4: Speciation of oxalic acid and conjugate oxalates as a function of pH using acid
1026 dissociation constant K1 = $5.9*10^{-2}$ and K2 = $6.4*10^{-5}$ (Chi and Xu, 1998).

1027

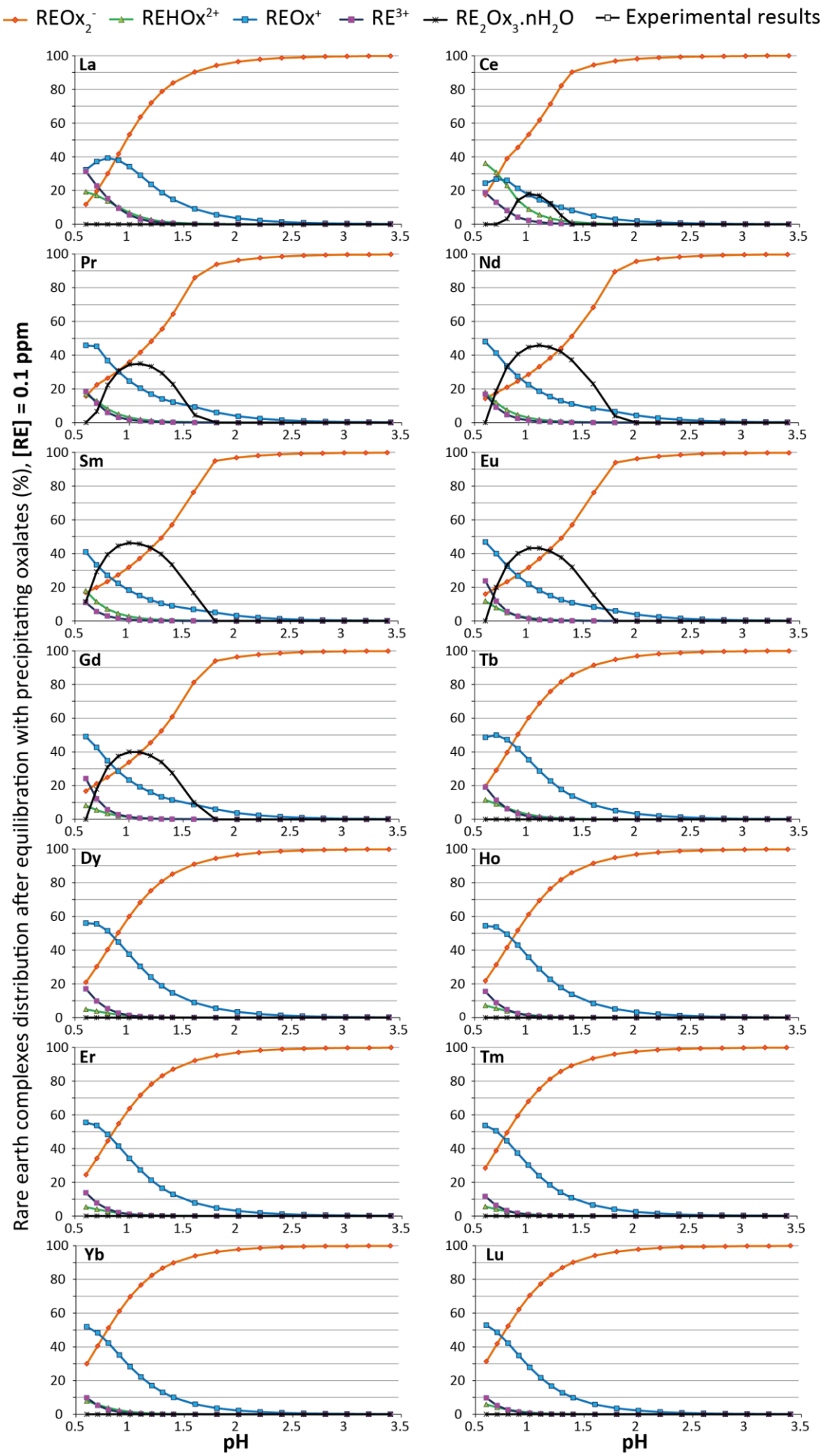

Supplementary Figure 5: REE speciation as a function of pH, [RE] = 0.1 ppm.

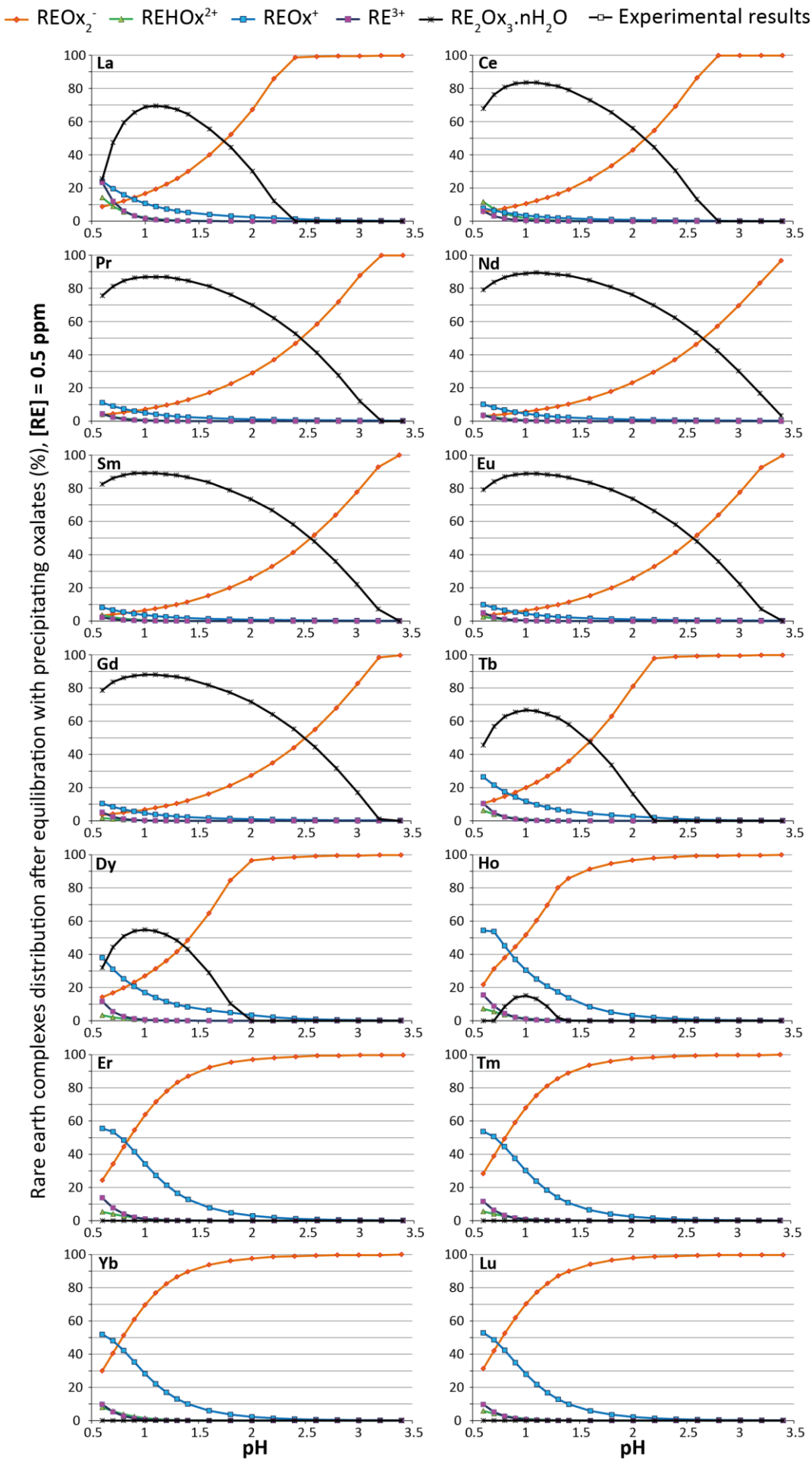

Supplementary Figure 6: REE speciation as a function of pH, [RE] = 0.5 ppm.

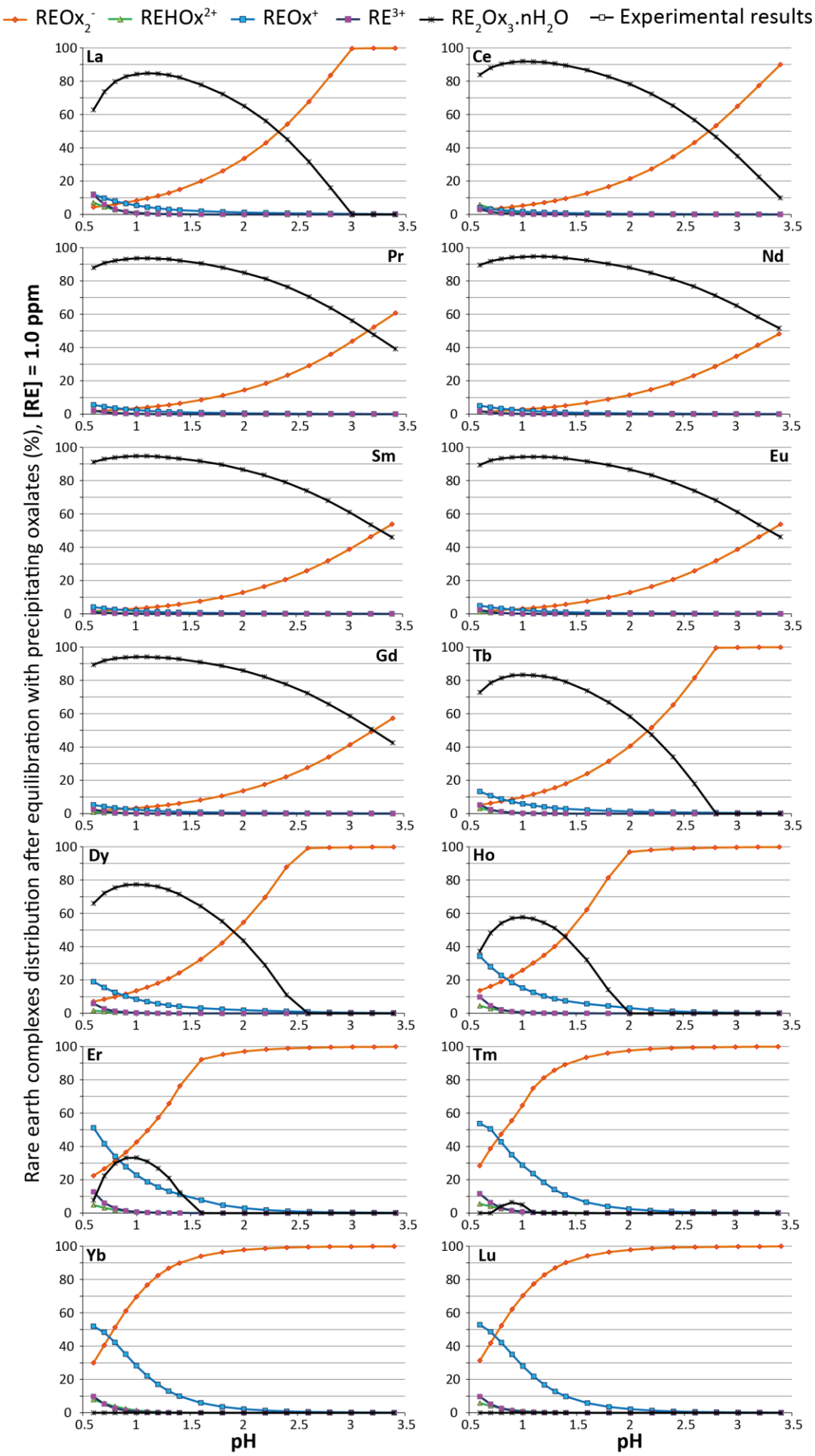

Supplementary Figure 7: REE speciation as a function of pH, [RE] = 1.0 ppm.

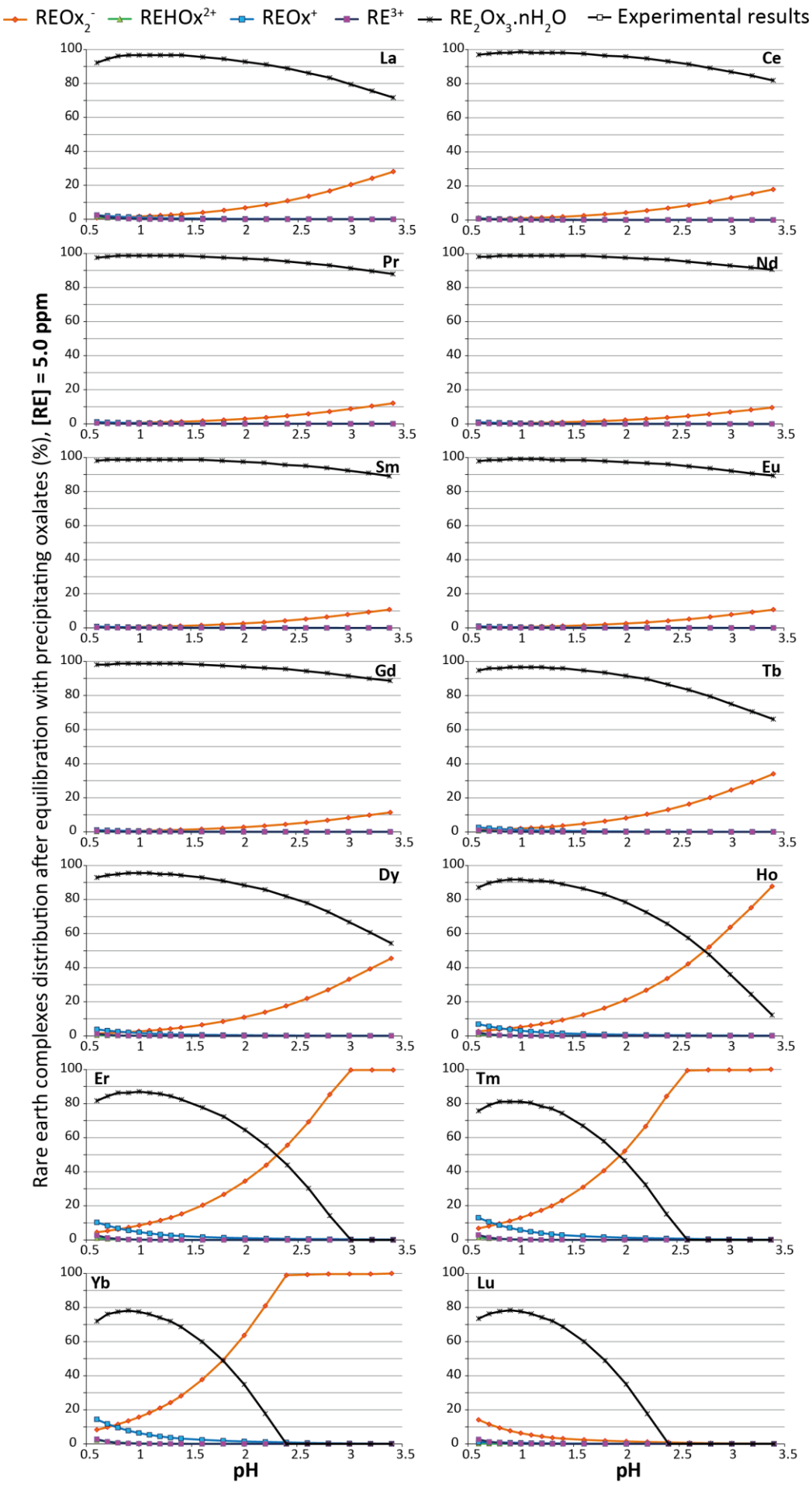

Supplementary Figure 8: REE speciation as a function of pH, [RE] = 5.0 ppm.

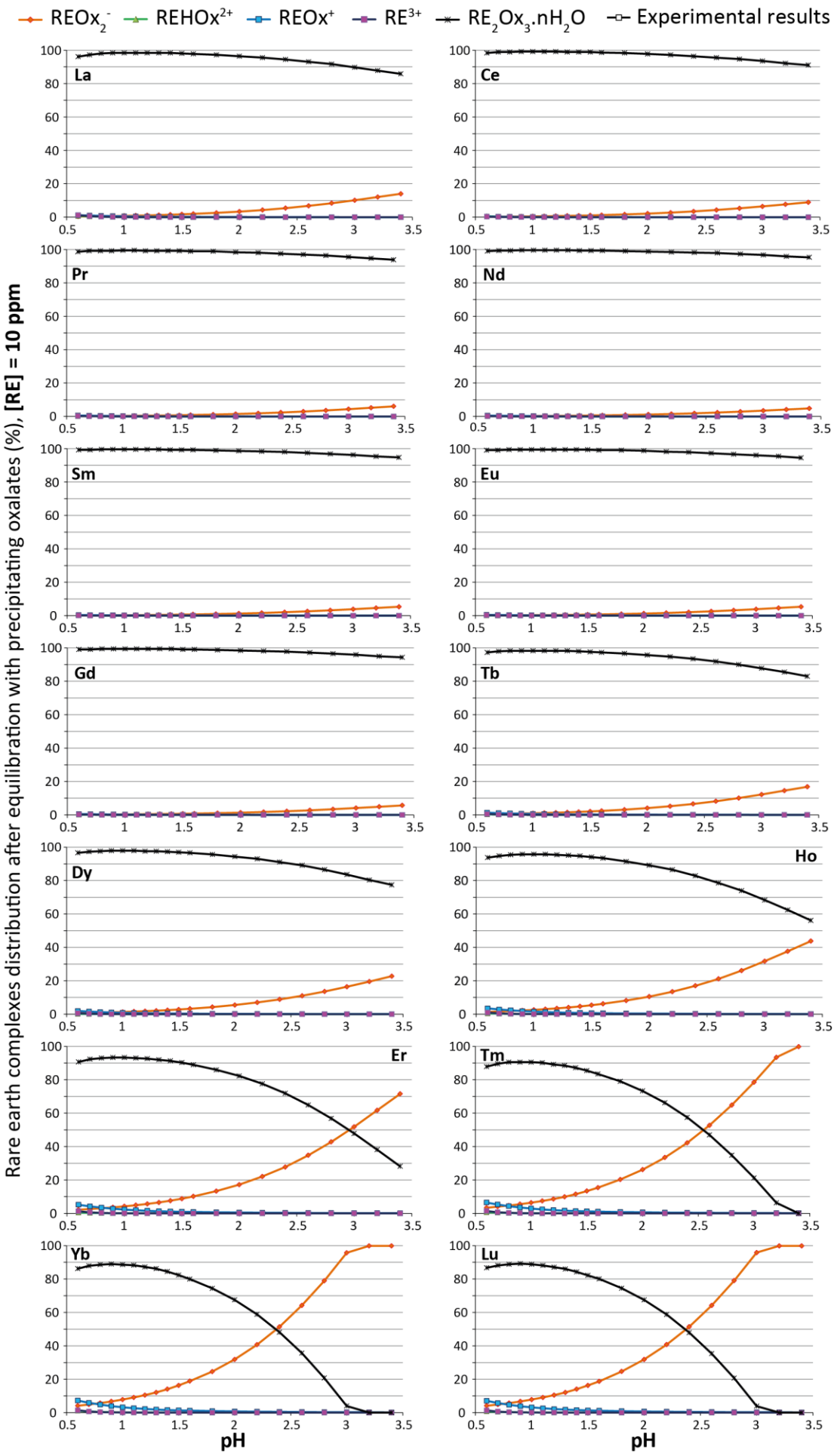

Supplementary Figure 9: REE speciation as a function of pH, [RE] = 10 ppm.

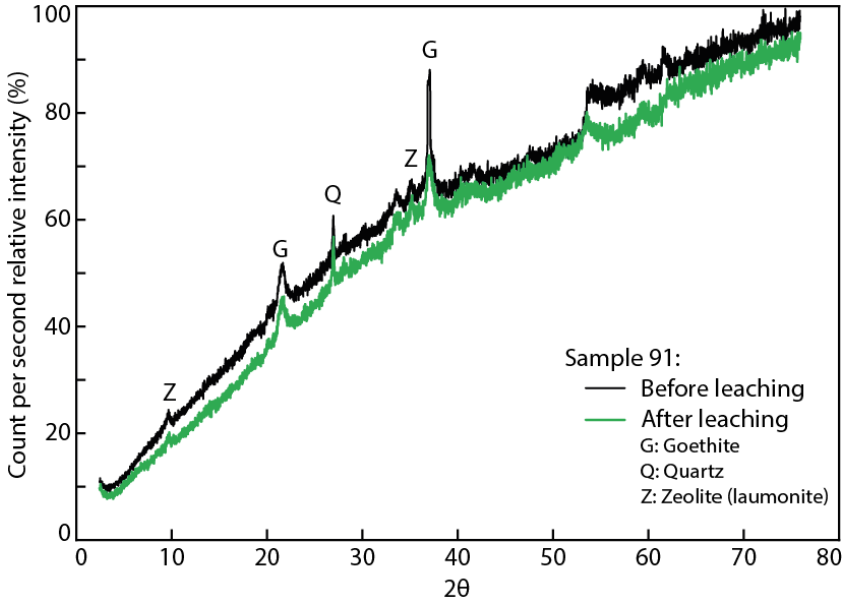

1038

1039 Supplementary Figure 10: Comparison of X-ray diffraction patterns of sample PJ-CY-2014-91 and the residue
1040 collected after filtration of the leaching experiment using 1M HCl at a liquid to solid ratio of 25, 20°C for 2h.

1041

1042